IMPROVING THE CONTROL OF TWO-MODE FLEXIBLE SYSTEMS WITH INPUT SHAPING

A Thesis
Presented to
The Academic Faculty

by

Raymond Charles Manning

In Partial Fulfillment
of the Requirements for the Degree
Master of Science in the
School of Mechanical Engineering

Georgia Institute of Technology
May 2008

IMPROVING THE CONTROL OF TWO-MODE FLEXIBLE SYSTEMS WITH INPUT SHAPING

Approved by:

Professor William Singhose,
Committee Chair
School of Mechanical Engineering
Georgia Institute of Technology

Professor Aldo Ferri
School of Mechanical Engineering
Georgia Institute of Technology

Professor Wayne Book
School of Mechanical Engineering
Georgia Institute of Technology

Date Approved: March 12, 2008

ACKNOWLEDGEMENTS

Many people have helped me complete this thesis. I would like to thank my advisor Dr. Singhose. His direction and willingness to help workout any problem that arose in my research is what has allowed me to bring this work to a successful conclusion. I would like to thank all my lab-mates for their help in running studies, proof reading papers, and always being willing to lend a hand. I would to thank Dr. Book for the use of RALF and Dr. Ferri for helping me with my dynamic analysis.

I am extremely grateful for the love and support of all my friends and family, my parents Holly and Hugh who were always there to support, listen, and nudge me in right direction, and my Grandmother Arlene, whose help allowed me to focus on my studies.

Finally, I thank our Heavenly Father for the strength, intelligence, and endurance to complete this thesis.

TABLE OF CONTENTS

LIST OF TABLES

LIST OF FIGURES

SUMMARY

Machine vibration leads to lower precision, efficiency, and safety. As a result, large sums of money and innumerable man-hours are spent in efforts to reduce vibration in machinery. A subclass of machinery that is widely used in industry is two-mode flexible systems. Cranes with double-pendulum dynamics and two-link flexible robotic arms are representative examples of two-mode flexible systems.

In order to thoroughly understand these types of systems, a detailed study of double-pendulum cranes is preformed. The crane payload is considered to be a distributed mass. The parameters of the payload and the crane has important effects on the dynamic response. the effects are studied as a function of the parameters so that effective control methods can be developed.

This thesis develops a technique for improving the control of two-mode flexible systems called input shaping. Input shaping is a control strategy that uses a series of impulses to modify the reference command to suppress unwanted vibration in a system. This thesis reviews several types of input shapers and presents a method for optimizing a robust input shaper called Specified Insensitivity input shapers using knowledge of amplitude contributions of each mode to the overall response. Simulations and experiments are presented to verify the new algorithm.

Two human operator studies are presented to demonstrate the effectiveness of input shaping when used in conjunction with distributed crane payloads, such as cargo containers. One study investigates the improvement in efficiency when using input shaping and the differences in efficiency between input shapers. The other study investigates operator learning when moving a payload with unshaped and shaped commands.

CHAPTER I

INTRODUCTION

All machines vibrate when they operate near their performance limit. These vibrations result in reduced precision, inefficiency, and more dangerous work environments. Whether it is a shipyard crane moving cargo containers or an industrial robot used in part-placement operations, a massive investment in man-hours and money is invested each year to reduce the vibrations inherent in machinery through vibration-suppressing controller design and operator training.

A subclasses of these machines are two-mode flexible systems such as double-pendulum cranes and two-link flexible robotic manipulators. When working with these systems, the changing payloads and configurations change the frequencies of oscillation. This creates the need for multiple payload considerations, increased workspace constraints, very robust control systems, and highly trained machine operators. In the case of cranes, skilled crane operators are required to keep the crane from becoming a hazard to those working with or around the payload. Large variation in payloads and operating parameters make classical feedback control difficult to implement on cranes. Furthermore, any computerized feedback controller can conflict with the human operator (who is also a feedback control system). Operators accrue years of experience to skillfully perform the required crane operations with varying payloads.

Usually robotic manipulators are very stiff in an effort to reduce the vibration in the system. However, this stiffness tends to slow the robot down. Flexible robotic manipulators have a limited use in industry because their flexible links are prone to large amounts of vibration. There is a large dominant mode of vibration always in

the system but certain configurations excite a second mode of vibration that becomes detrimental to the performance. Therefore, the workspace of a robot may be limited to reduce the areas in which large amounts of vibration may affect the operation of the robot. Controllers on robotic manipulators can be very complicated and involve non-linear control elements and gain scheduling to increase the robustness of the system when moving payloads in pick-and-place operations. This results in high development and implementation costs.

1.1 Thesis Overview

This thesis will investigate the control of two-mode flexible systems using input shaping techniques. Chapter 1 will focus on explaining the technique of input shaping. The concept of input shaping will first be explained and a review of previously developed input shapers will be provided. Chapter 2 will introduce an in-depth dynamic analysis of bridge cranes with distributed payloads. This chapter will investigate the effects of various system properties on the system frequencies and amplitudes contributions of these frequencies to the system response. Chapter 3 will review a robust input-shaping technique called Specified Insensitivity (SI) input shaping and introduce a constraint equation optimization technique called Varying Amplitude Contribution Specified Insensitivity (VACSI) input shaping. Chapter 4 will present experimental results of VACSI input shapers on a 10-ton industrial bridge crane and a flexible robotic arm. Chapter 5 will investigate human operation of industrial bridge cranes. Two studies are presented. The first study investigates how different input shapers improve crane operator efficiency when moving distributed payloads. The second study investigates operator learning with and without input shaping. Finally, Chapter 6 will discuss future work and present the conclusions drawn from this thesis.

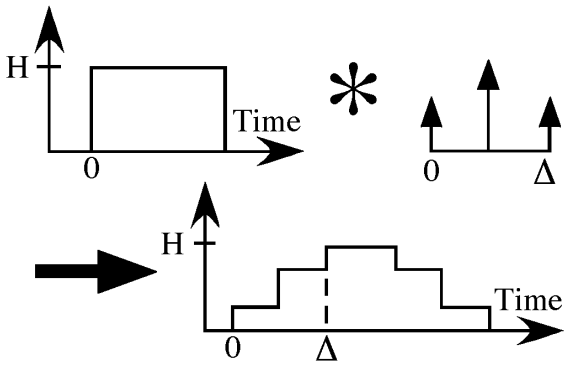

Figure 1: Input Shaping Process

1.2 Input Shaping

Input shaping is a form of system control that modifies the reference command to suppress vibration as seen in Figure 1. A reference signal is convolved with a series of impulses, called the input shaper, and results in a specially shaped reference command that suppresses the vibration in the system. The input shaper is designed to suppress the system vibration at a specified design frequency, ω. The resulting shaped command is then used to move the system without exciting the offending frequency. An early form of input shaping was developed in the 1950's by O.J.M. Smith known as posicast control [61]. Posicast control was not widely used because it lacked robustness and it was difficult to implement without a digital computer [64]. An example shaped command and system response is shown in Figure 2. In this example, the design frequency is 1 Hz. When using an input shaper, the command is extended by the duration of the shaper, in this example, 0.5 seconds. This results in a longer rise time, but also results in a faster settling time because the residual vibration is eliminated.

Input shapers are designed using constraint equations developed to limit the amount of residual vibration in the system using frequency and damping ratio information [49, 36]. Vibration constraints, impulse amplitude constraints, robustness constraints, and shaper duration minimization constraints are all utilized to design

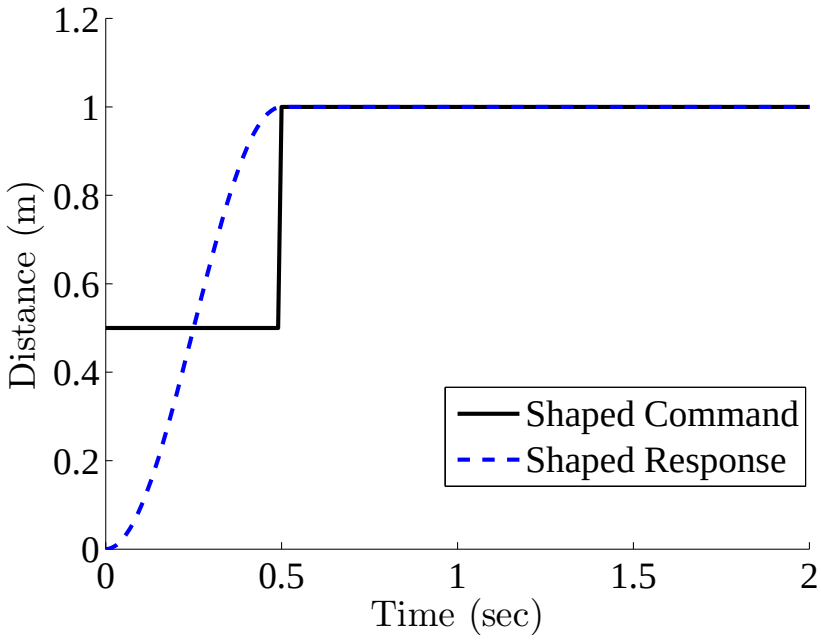

Figure 2: Shaped Input and Response

an input shaper.

To develop the vibration constraint equation, the amplitude of the response of a second-order harmonic oscillator to a series of impulses is examined [6]:

$$A_{\sum} = \frac{\omega}{\sqrt{1-\zeta^2}} e^{-\zeta\omega t_n} \sqrt{[C(\omega,\zeta)]^2 + [S(\omega,\zeta)]^2}, \tag{1}$$

where,

$$C(\omega,\zeta) = \sum_{i=1}^{n} A_i e^{-\zeta\omega t_i} \cos(\omega_d t_i), \tag{2}$$

$$S(\omega,\zeta) = \sum_{i=1}^{n} A_i e^{-\zeta\omega t_i} \sin(\omega_d t_i), \tag{3}$$

$$w_d = w_n \sqrt{1-\zeta^2}. \tag{4}$$

These equations describe the amplitude of the vibration remaining in the system after a series of impulses. In order to express the amplitude in a non-dimensional form, (1)

is divided by the residual amplitude of the response to a single impulse, $A_{\uparrow}$:

$$A_{\uparrow} = \frac{\omega}{\sqrt{1-\zeta^2}} \tag{5}$$

The resulting equation gives the residual vibration in a system as a percentage of the shaped vibration divided by the unshaped vibration:

$$V(\omega,\zeta) = e^{-\zeta\omega t_n}\sqrt{[C(\omega,\zeta)]^2 + [S(\omega,\zeta)]^2} \tag{6}$$

For the design of Zero Vibration (ZV) input shapers, (6) is set to zero. ZV shapers create an impulse sequence that causes no residual vibration in the system after the completion of the move. ZV shapers have poor robustness to modeling errors and noise. To add robustness, the derivative of (6) can also be set to zero, creating a ZVD shaper [49]:

$$0 = \frac{\partial}{\partial\omega}[e^{-\zeta\omega t_n}\sqrt{[C(\omega,\zeta)]^2 + [S(\omega,\zeta)]^2}] \tag{7}$$

The trade off for adding this constraint is a longer shaper duration, and hence command rise time.

Sensitivity plots for ZV and ZVD shapers are shown in Figure 3. This plot shows how percent residual vibration, (6), from an input-shaped command is affected by a deviation in the actual system frequency, ω_m, from the design frequency, ω. If 5% of the residual vibration without input shaping is considered acceptable, then the insensitivity, I, is defined as the width of the curve that lies below this tolerable vibration level. From the figure, it can be seen that ZV input shapers have a very small insensitivity, 0.06 ($\pm$3%), around the modeled frequency, ω_m. By enforcing (7), the insensitivity increases to 0.29 ($\pm$14.5%). Because the vibration is measured as a percentage, this plot works for any reference command. More robust input shapers and a more in depth review of input shaper constraint equations is presented in Chapter 3.

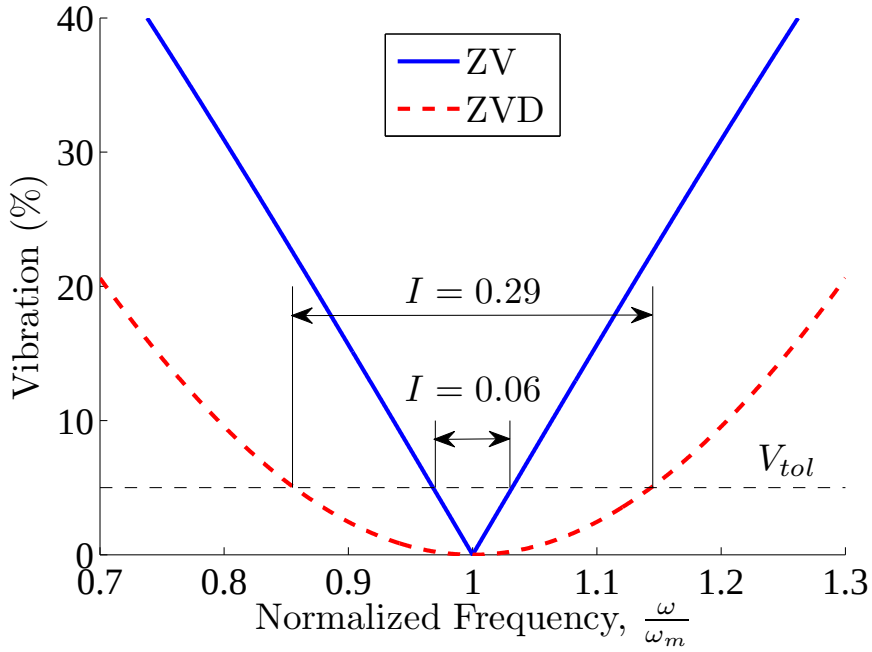

Figure 3: ZV and ZVD Sensitivity Plot

While input shaping will be used in this thesis to control systems, other command-shaping techniques have been developed and some are mentioned here. Many researchers have used various filtering techniques such as notch filters to suppress the vibration in a system [14, 66]. Rhim and Book developed an adaptive Time-Delay command-shaping technique to cancel vibrations in flexible manipulators [8, 43]. Auernig and Troger developed time-optimal commands to move overhead cranes with hoisting [1].

Input shaping has been successfully used to control many types of systems. Input shaping was used to suppress hook swing in cranes in [24, 51, 55, 56, 59]. Flexible robotic manipulators were controlled using input shaping in [16, 33, 34, 44]. Commands were modified using input shaping in [2, 65] to control flexible spacecraft.

1.3 Thesis Contributions

The contributions of this thesis are:

1. An in-depth dynamic analysis of bridge cranes with distributed payloads. The

effects of cable lengths, hook and payload mass, and payload geometry on the system frequencies and their amplitude contributions are presented.

2. An algorithm for optimizing Specified Insensitivity input shaper constraint equations, called Varying Amplitude Contribution SI input shaping. By varying the vibration constraint equations to account for the amplitude contributions of each frequency mode, shaper duration can be reduced, thereby allowing for faster rise times.

3. Input shaping is shown to immediately improve operator efficiency when moving distributed payloads. It is shown that operators learn how to control the payload over time when not using input shaping, but can not achieve the efficiency of novice operators using input shaping.

CHAPTER II

DYNAMICS OF DISTRIBUTED PAYLOAD CRANES

In order to apply multiple-mode vibration suppression using input shaping to cranes, the dynamics of a crane with a distributed payload must be understood. Past researchers have worked on suppressing vibration on bridge an tower cranes that act as double pendulums with a point mass payload [23]. Unfortunately, many payloads in industrial settings do not act as simple point masses; but rather as distributed solid bodies. Examples of such payloads include munitions and ship cargo containers. These bodies require that the inertia of the payload be considered in the dynamic analysis of the crane. The purpose of this chapter is to analyze the dynamics of a crane with a distributed payload. To accomplish this, a new model for a crane with a disturbed payload was created and simulations and experiments were conducted to verify that the equations accurately represent actual crane dynamics. Analysis of the crane response with different payloads and varying cable lengths was conducted in order to understand how input shaping could best be applied to the system.

2.1 Crane Model

The model under consideration is shown in Figure 2.1. Equations of motion were created using the dynamic modeling program Autolev [22]. The model consists of a trolley rolling on a bridge with a hook suspended by a massless cable. The hook is modeled as a point mass with mass, m_h. The distance from the trolley to the hook is the suspension length, L_c. Attached to the hook is a generalized payload. The payload is characterized by its mass, m_p, the distance from the hook to the center of mass of the payload called the rigging length, L_r, and the radius of gyration of the payload, κ. The center of mass is assumed to hang below the hook when the system

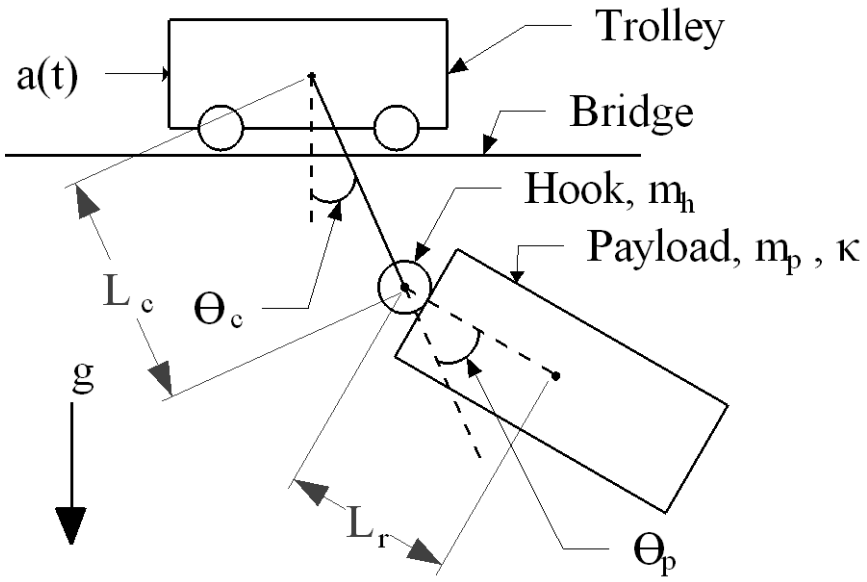

Figure 4: Crane Model with Generalized Payload

is at rest. The input to the system is an acceleration of the trolley, $a(t)$. The cable is assumed to be massless. No damping or friction is assumed for this model. The variables of interests are the swing angle of the cable, θ_c, and the swing angle of the payload, θ_p.

2.2 Equations of Motion

The model results in the following non-linear equations of motion:

$$\begin{aligned} 0 = & - gL_c m_h \sin(\theta_c) - L_c m_h a(t)\cos(\theta_c) - gm_p(L_c \sin(\theta_c) + L_r \sin(\theta_c + \theta_p)) \\ & - m_p(L_c a(t)\cos(\theta_c) + L_r a(t)\cos(\theta_c + \theta_p) + L_c L_r \sin(\theta_p)\dot{\theta_c}^2 \\ & - L_c L_r \sin(\theta_p)(\dot{\theta_c} + \dot{\theta_p})^2) - (m_p\kappa^2 + L_r m_p(L_r + L_c\cos(\theta_p)))\ddot{\theta_p} \\ & - (m_p\kappa^2 + m_h L_c^2 + m_p(L_c^2 + L_r^2 + 2L_c L_r \cos(\theta_p)))\ddot{\theta_c} \end{aligned} \tag{8}$$

$$\begin{aligned} 0 = & - L_r m_p(g\sin(\theta_c + \theta_p) + a(t)\cos(\theta_c + \theta_p) + L_c \sin(\theta_p)\dot{\theta_c}^2) \\ & - (m_p\kappa^2 + m_p L_r^2)\ddot{\theta_p} - (m_p\kappa^2 + L_r m_p(L_r + L_c\cos(\theta_p)))\ddot{\theta_c} \end{aligned} \tag{9}$$

In order to find closed-form solutions for the system oscillation frequencies the equations must be linearized. To linearize the equations, two assumptions are made:

- Small Angles
- Small Angular Velocities

Because the swing angles of a crane cable or payload rarely grow larger than 15 degrees, the small angle assumption works well. It can be assumed that the crane will operate relatively slowly, thus allowing for the $\dot{\theta}^2$ terms to be neglected. The resulting linearized equations of motion are:

$$\begin{aligned}&(m_p\kappa^2 + L_r m_p(L_r + L_c))\ddot{\theta_p} + (m_p\kappa^2 + m_h L_c^2 + m_p(L_c^2 + L_r^2 + 2L_c L_r))\ddot{\theta_c} \\ &= -(gL_c m_h + gm_p L_c + gm_p L_r)\theta_c - (gm_p L_r)\theta_p - (L_c m_h + m_p(L_c + L_r))a(t) \end{aligned} \quad (10)$$

$$\begin{aligned}&(m_p\kappa^2 + m_p L_r^2)\ddot{\theta_p} + (m_p\kappa^2 + L_r m_p(L_r + L_c))\ddot{\theta_c} \\ &= -L_r m_p g\theta_c - L_r m_p g\theta_p - L_r m_p a(t) \end{aligned} \quad (11)$$

Converting the equations to the Laplace domain, setting the mass ratio $R = \frac{m_p}{m_h}$, and separating the states to be independent of each other yields:

$$\frac{\Theta_c}{A} = \frac{-(s^2(L_r^2 + \kappa^2(R+1)) + gL_r(R+1))}{(L_c(L_r^2 + \kappa^2(R+1))s^4 + g(R+1)(\kappa^2 + L_r L_c + L_r^2)s^2 + g^2 L_r(R+1))} \quad (12)$$

$$\frac{\Theta_p}{A} = \frac{(L_r^2 + \kappa^2(R+1))s^2}{(L_c(L_r^2 + \kappa^2(R+1))s^4 + g(R+1)(\kappa^2 + L_r L_c + L_r^2)s^2 + g^2 L_r(R+1))} \quad (13)$$

Where Θ_c is the Laplace transform of θ_c, Θ_p is the Laplace transform of θ_p, and A is the Laplace transform of $a(t)$.

2.3 Frequencies

The system is a two-mode system, with two distinct frequencies, and therefore can be expressed as the sum of the two frequency contributions. To do this the two

frequencies need to be isolated. By solving the denominator of (12) and (13) for s^2, and then solving $(s^2 + \omega^2) = 0$ for ω^2, the frequencies can be determined, as:

$$\omega_1^2 = \frac{g(R+1)}{(2L_c)}(\alpha - \beta) \tag{14}$$

$$\omega_2^2 = \frac{g(R+1)}{(2L_c)}(\alpha + \beta) \tag{15}$$

Where,

$$\alpha = \frac{\kappa^2 + L_r L_c + L_r^2}{L_r^2 + \kappa^2(R+1)} \tag{16}$$

$$\beta = \sqrt{\alpha^2 - \frac{4L_r L_c}{(R+1)(L_r^2 + \kappa^2(R+1))}} \tag{17}$$

Figure 5 shows how the first frequency of the crane with various payloads changes if the total length from the payload and cable, L_t, is held constant while the rigging length, L_r is varied. The mass of the payload, m_p, and the radius of gyration, κ, are also varied, while the hook mass, m_h is held constant. A point mass is represented by a radius of gyration, $\kappa = 0$. Figure 6 shows how the second frequency of the crane is affected by changing the rigging length, radius of gyration and the payload mass. The larger radii can represent any payload from shipping containers to building support beams depending on where the payload is attached to the hook. Table 1 shows the median value of the two frequencies and how they vary over the range of rigging lengths, radii of gyration, and payload masses. This table shows that for small radii of gyration, less than or equal to 1, the low-mode frequency does not vary much from the median value, but as the radius of gyration increases, the low-mode frequency starts to vary a great deal when the rigging length and payload masses are changed. Conversely, The high-mode frequency varies a great deal regardless of the payload's radius of gyration.

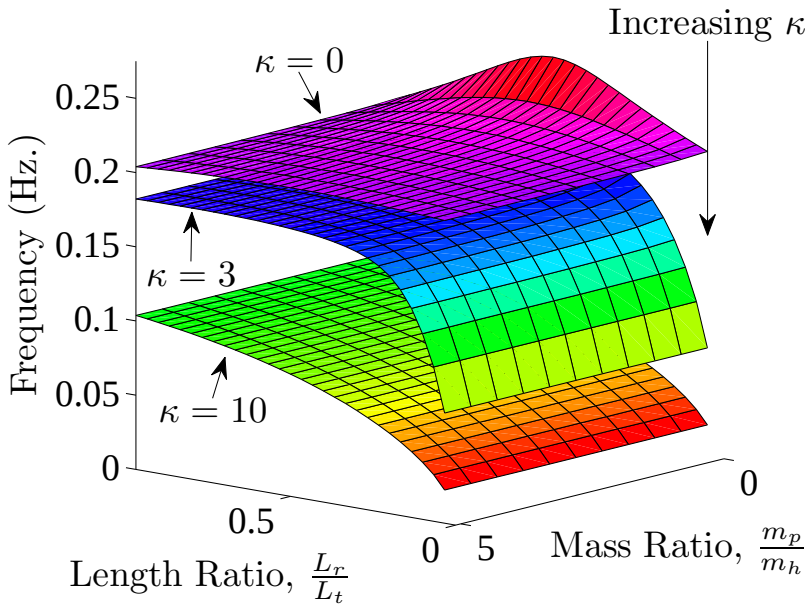

Figure 5: Low-Mode Frequencies for Various Radii of Gyration

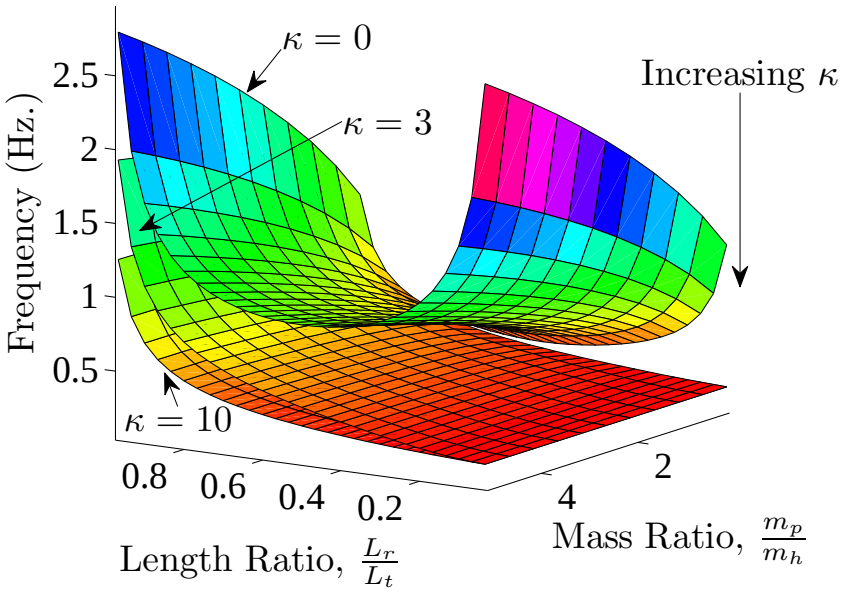

Figure 6: High-Mode Frequencies for Various Radii of Gyration

Table 1: Frequency Ranges for a Variety of Payloads

Radius of Gyration	Mode	Median Frequencies (Hz.)	Variation
0	Low	0.23	± 11%
	High	1.57	± 78%
1	Low	0.22	± 12%
	High	1.42	± 84%
5	Low	0.10	± 56%
	High	0.88	± 77%
10	Low	0.06	± 65%
	High	0.73	± 73%
50	Low	0.01	± 68 %
	High	0.67	± 69 %

2.3.1 Effect of Payload Mass

In order to generate the data in Figures 6 and 5 the mass of the payload was varied from about 20% of the mass of the hook to 500%. Over most of the range, the mass of the payload has little effect in the changing the low-mode frequency, as shown in Figure 5. Only when the payload mass is small compared to the hook mass and when the rigging and suspension length are roughly equal does the mass of the payload change the frequency a great deal.

The high-mode frequency is affected by the mass of the payload much more. For small radii of gyration, increasing the mass of the payload substantially increases the high-mode frequency. These results correspond well to the double-pendulum frequencies that arise from a point mass payload. As the radius of gyration increases, the effect of the mass on the frequency decreases.

2.3.2 Effect of Rigging Length

The rigging length was varied between 3% of the total length of the system to 97% of the total length. For most of the range, the low-mode frequency is affected very little by the rigging length. The rigging length has a larger effect on the frequency when the rigging length is small and the suspension length is large. Conversely, the

high mode is affected by the rigging length over the whole range. As the radius of gyration increased, the effect of the rigging length decreases for both frequencies.

2.3.3 Effect of Radius of Gyration

When the radius of gyration is small, the high-mode frequency is high. As the radius of gyration increases, the frequency decreases, moving closer to the low-mode frequency. The frequency range for the high frequency of the two-mode crane system is large, varying upwards of ±84% as a function of the mass and length ratios at a radius of gyration of 1 m. The low frequency does not vary a great deal for small radii of gyration, only ±12%. As the radius of gyration increases, the low frequency decreases, and the range that the frequency may vary increases to ±68%.

To demonstrate how the radius of gyration affects the frequencies in more detail, Figure 7 shows the frequencies when the radius gyration and the rigging length change. The total length of the system is held constant. Since the mass of the payload affects the system to a smaller degree than the rigging length or the radius of gyration, it is held constant with a mass ratio set equal to 1.

When the rigging length is small, the frequencies are close together, but they separate as the rigging length increases. The radius of gyration changes the frequencies a great deal when it is small but as it increases in value, the frequency changes less with the changing radius of gyration. This effect can be seen also in (16) and (17). As κ increases, it dominates both equations causing $\alpha \to 1$ and $\beta \to \alpha$. This in turn reduces the effect of κ the frequencies. The lengths have the larger effect on the frequencies at the extreme ends of the range because they dominate the equations when the radius of gyration is either very large ($\beta \to \alpha \to 1$) or is very small ($\kappa \ll L_c, L_r$).

2.4 Amplitude Contribution

The effect of changing the payloads radius of gyration and the rigging length on the frequency values is large, but how does this affect the overall response of the system?

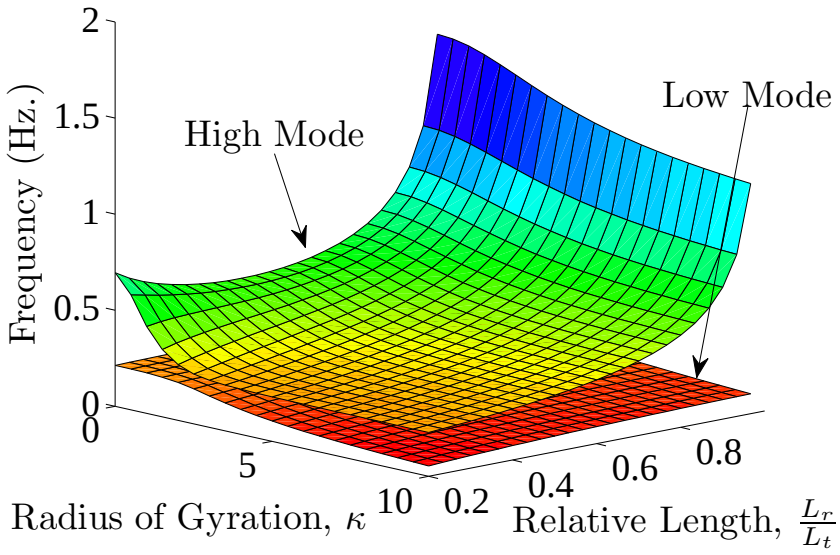

Figure 7: Frequencies for A Range of Length Ratios and Radii of Gyration

When moving payloads with a crane, small amplitude oscillations, such as 2 cm, are insignificant. Therefore, their impact on the control and positioning of the crane do not justify the cost of designing a control system to minimize these portions of the response. As a result, it is important to assess the amplitude contributions of the two frequencies to the overall position response of the crane.

Taking the frequencies in (14) and (15) and plugging them into the Laplace domain equations of motion give:

$$\frac{\Theta_c}{A} = \frac{-1}{L_c(L_r^2 + \kappa^2(R+1))} \frac{\frac{s^2}{L_c} + gL_r(R+1)}{(s^2+\omega_1^2)(s^2+\omega_2^2)} \tag{18}$$

$$\frac{\Theta_p}{A} = \frac{\frac{s^2}{L_c}}{(s^2+\omega_1^2)(s^2+\omega_2^2)} \tag{19}$$

Using an impulse of magnitude, A, as the input and converting (18) and (19) to the time domain give the impulse response:

$$\theta_c = A\frac{\omega_1(1+\omega_2^2 L_r\gamma)}{g\beta(R+1)}\sin(\omega_1 t) - A\frac{\omega_2(1+\omega_1^2 L_r\gamma)}{g\beta(R+1)}sin(\omega_2 t) \tag{20}$$

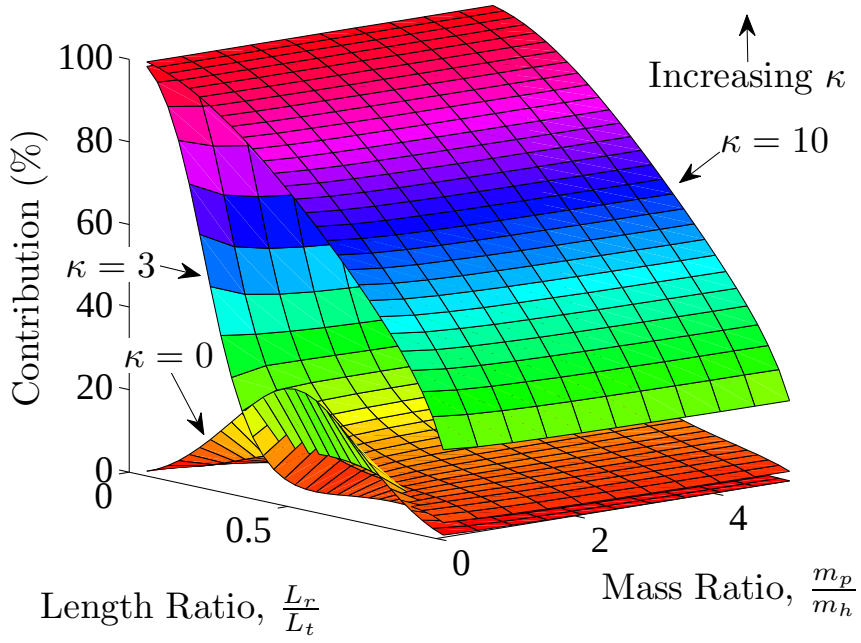

Figure 8: High-Mode Amplitude Contributions to Overall Response

$$\theta_p = A\frac{-\omega_1}{g\beta(R+1)}\sin(\omega_1 t) + A\frac{\omega_2}{g\beta(R+1)}\sin(\omega_2 t) \tag{21}$$

Where,

$$\gamma = \frac{-g(R+1)}{\omega_1^2\omega_2^2(L_r^2 + \kappa^2(R+1))} \tag{22}$$

The horizontal motion of the payload is:

$$x(t) = L_c\sin(\theta_c) + L_r\sin(\theta_c + \theta_p) \tag{23}$$

If small angles are assumed, then the horizontal payload motion is:

$$x(t) = A\frac{L_c + \omega_2^2 L_r\gamma(L_c + L_r))}{g\beta(R+1)}\omega_1\sin(\omega_1 t) - A\frac{L_c + \omega_1^2 L_r\gamma(L_c + L_r)}{g\beta(R+1)}\omega_2\sin(\omega_2 t) \tag{24}$$

This expression gives the response as uncoupled contributions from the two frequencies. By extracting the coefficients of the *sin* terms, the contributions of the two frequencies can be compared to ascertain whether both frequencies need to be accounted for in the design of the control system. Figure 8 shows the level of contribution of the high-mode frequency to the overall response with various payloads, defined by

Table 2: Amplitude Contributions for Variety of Payloads

Radius of Gyration	Mode	Median Amplitude Contributions (%)	Variation
0	low	86%	± 62%
	high	14%	± 9%
1	low	86%	± 63%
	high	14%	± 10%
5	low	47%	± 459%
	high	53%	± 53%
10	low	40%	± 636%
	high	60%	± 55%
50	low	20%	± 1369%
	high	80%	± 29%

their radius of gyration. The amplitude contribution is defined as the amount of the response a given frequency contributes to the overall impulse response. The vertical axis shows the level of contribution as a percentage the total response. The horizontal axes show how the payload properties, rigging length, L_r, and payload mass, m_p, affect the contributions. The low-mode frequency contribution is the total response minus the contribution level shown in the figure. Table 2 shows the variation of the amplitude contributions around the median value for a given payload's radius of gyration. The first two columns of the table gives the radius of gyration and which frequency mode is contributing to the response. The third column shows median amplitude contributions as a percentage of the total response. The fourth column shows how much the amplitude contribution from each frequency can vary over the range of relative lengths and masses used in Figure 8. It can be seen from the table that the contributions can range a great deal for all the payloads.

2.4.1 Effect of Payload Mass

The mass does not have a large effect on the contribution of the low-mode frequency to the overall response when the mass ratio is larger than 0.5, meaning that the mass of the payload is half the mass of the hook. The mass becomes a larger factor in

the amplitude contribution only when the mass ratio becomes smaller than 0.5. The effect of the hook and payload masses on the high-mode frequency contribution, when the mass ratio is less than 0.5, decreases as the radius of gyration increases, as shown in Figure 8.

2.4.2 Effect of Rigging Length

The rigging length has a large effect on the contributions of the different frequencies to the overall response of the system. For small radii of gyration, the effect of the rigging length is most pronounced when the rigging length and suspension length are approximately equal. This is consistent with findings of early researchers who investigated point-mass double-pendulums [55]. As the radius of gyration increases, the entire range of rigging lengths become important to the overall amplitude contribution. When the rigging length is small, or the suspension length dominates the total length of the system, the amplitude contribution changes drastically as the radius of gyration increases. This shows that the rigging length has a large influence on the amplitude contribution as the radius of gyration increases.

2.4.3 Effect of Radius of Gyration

The radius of gyration greatly affects the amplitude contributions of each mode. When the radius of gyration is small, the contribution of the low-mode to the overall response is dominant. As the radius of gyration increases, the contribution of the high mode frequency becomes more important. At large radii of gyration, the contribution of the low mode diminishes for the entire range of payload masses. The contribution only increases when the rigging length becomes longer.

Figure 9 shows how the radius of gyration affects the amplitude contributions of each mode in more detail. Because the mass of the payload does not contribute to the overall response as much as the rigging length and the radius of gyration, the mass ratio for Figure 9 was held constant at 1. For small radii of gyration, the high-mode

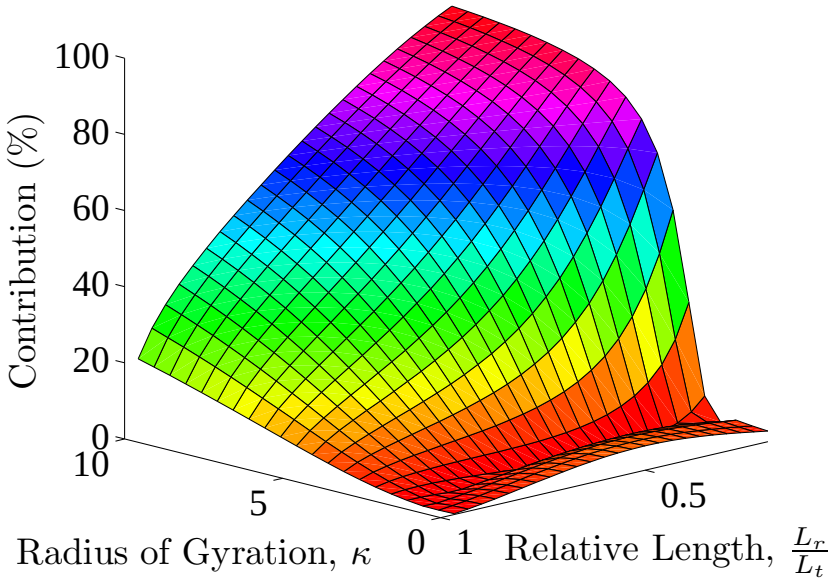

Figure 9: Amplitude Contribution of High Mode to Varying Radii of Gyration

frequency contributes very little to the system response. The rigging length does little to affect the level of contribution in this range. As the radius of gyration increases, its effect on the amplitude contribution of the high-mode increases. The reason for this is because as the radius of gyration is increasing, the moment of inertia is also increasing. As the inertia of the system grows, it becomes more resistant to motion. This causes the payload to oscillate less around the hook, resulting in a smaller amplitude contribution. Therefore, the high-mode frequency becomes the frequency that dominates the system response. The rigging length becomes the dominant factor as the radius of gyration increases.

2.5 Summary

The dynamics of the distributed payload crane are dependent on the payload mass, rigging length, and radius of gyration of the payload. The payload mass significant effect on the system frequencies and amplitude contributions when the mass of the payload is small relative to the mass of the hook and the radius of gyration is small.

The radius of gyration has a large effect on the frequencies and the amplitude contributions when it is small but becomes less dominant as it increases. The rigging length has the largest influence on both the frequencies and the amplitude contributions when the radius of gyration grows large, higher than approximately 5 meters, such as with a cargo container. The suspension length also has a large influence on the frequencies and amplitude contributions.

Based on the dynamic properties summarized above, the control of cranes with distributed payloads needs to focus on the effects of rigging length and the radius of gyrations on the overall response. By finding the ranges that the rigging length or suspension length and the radius of gyration will vary, a control scheme can be tailored to minimize the affects of the two modes of vibration.

CHAPTER III

ROBUST INPUT SHAPERS

In Chapter 1, input shaping was shown to suppress motion-induced vibrations by generating a command that cancels the problematic frequencies. Zero-Vibration (ZV) and Zero-Vibration and Derivative (ZVD) were shown to suppress the vibration in a system in a small and medium range around the design frequency, ω. Multiple modes of vibration could be suppressed by convolving multiple shapers together. The limitation of these shapers were shown to be their robustness to changing design frequencies. If the design frequency changes by more than the shaper's inherent insensitivity, then the input shaper was no longer able to suppress the vibration to the desired level. This chapter will review a robust input-shaping technique for suppressing vibration contributions from multiple modes of vibration called Specified Insensitivity (SI) input shaping [12, 55]. Algorithms will be presented for improving the design of SI shapers for use on two-mode systems.

3.1 Specified Insensitivity Input Shaping

Specified Insensitivity (SI) Input Shaping is a robust input-shaping technique that taylors the control robustness to suppress any desired range of frequencies.

3.1.1 Vibration Constraint

The vibration constraint limits residual vibration in the system. Where SI shaping differs from ZV and ZVD shapers is to what level of suppression and over what range of frequencies the residual vibration is suppressed. In ZV and ZVD shaper design, the residual vibration is set to zero at a single frequency, meaning there should be no vibration response from the system using the shaped input command. While

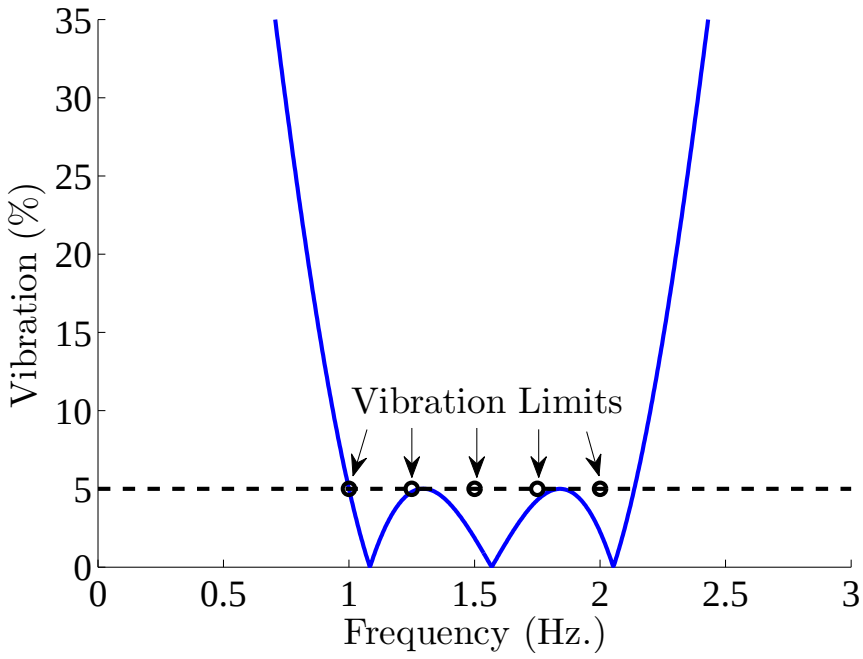

Figure 10: Vibration Suppression Constraints for SI Shapers

theoretically possible, in practice, this constraint is unattainable. It is possible to get close to zero vibration but to attain zero vibration is not possible. Model inaccuracies and noise are the main reasons why this constraint is not achievable in practice.

SI input shaping changes the vibration constraint to reflect reality that some small level of vibration will always exist and is tolerable. The residual vibration of the system, $V(\omega, \zeta)$, must be less than the vibration tolerance, V_{tol}:

$$V_{tol} \geq V(\omega, \zeta) \tag{25}$$

The vibration tolerance is often chosen around 5% of the unshaped amplitude, but it can be any value the designer wishes. When using this constraint, several versions of (25) are enforced throughout a frequency range to be sure that this constraint is enforced over a range of possible frequencies, as seen in Figure 10.

Many applications do not call for a reduction of vibration in the system response in percentage but rather in a measurable unit such as centimeters or inches. To account for this, the designer needs to measure the vibration in the system without input shaping and convert the desired response to a percentage of the original response.

3.1.2 Shaper Amplitude Constraints

Setting the residual vibration of the system below the tolerable level alone does not allow the designer to create an impulse sequence. Limitation must also be placed on the impulse amplitudes. The following constraint equation requires all the impulses in the input shaper to sum to 1:

$$\sum_{i=1}^{n} A_i = 1 \tag{26}$$

This constraint forces the output of the shaper (the shaped command) to reach the desired setpoint of the command being shaped. Simply enforcing the vibration constraint and the amplitude constraint would allow the resulting impulses to range from positive to negative infinity. This has the possibility of generating a shaped command that is not attainable by the system actuators. To eliminate this possibility, two different additional constraints can be enforced. One approach is to limit each impulse below some desired magnitude and allow negative impulses [58]. The second approach, and the one used in this chapter, is to require all the impulses to be positive:

$$A_i > 0, \;\; i = 0, ..., n \tag{27}$$

The techniques developed in this chapter can be extended to shapers containing negative impulses. There are drawbacks and possible issues with using that approach though. The biggest deterrent to using negative impulses is the risk of exciting and amplifying unmodeled high frequency modes in the system. The tradeoff for this risk is that negative impulses decrease rise time allowing for faster system response [58].

3.1.3 Duration Constraints

Using the above equations to produce an input shaper still allows for an infinite solution space. To find the fastest solution to the constraint equations, the shaper duration in minimized:

$$\min t_n \tag{28}$$

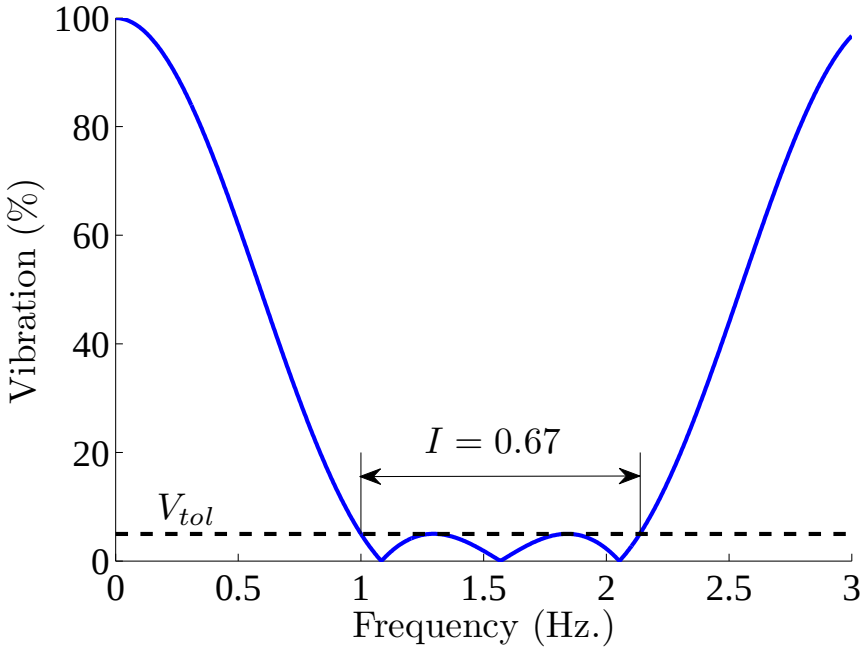

Figure 11: Sensitivity Curve for a SI Shaper

By enforcing a minimum time solution, the designer ensures that the input shaper will be fastest shaper possible given the constraints. The shapers designed for this thesis were generated by solving the above constraints using MATLAB's Optimization toolbox.

3.1.4 Robustness

The major drawback to using ZV input shapers is their sensitivity to modeling errors. While ZVD shapers are more robust, they do not allow for the insensitivity to be chosen. SI input shapers, by design, have a variable insensitivity that can be specified by the designer. Figure 11 shows an example of a sensitivity curve for a frequency suppression range between 1 Hz and 2 Hz. Insensitivity ranges are used when designing an SI shaper because the sensitivity plot is tailored to be robust over a desired frequency range. The design frequency found in the model can be anywhere in this frequency range, allowing the designer to expand one side of the suppression range to compensate for a larger variation in frequency to above or below the design frequency.

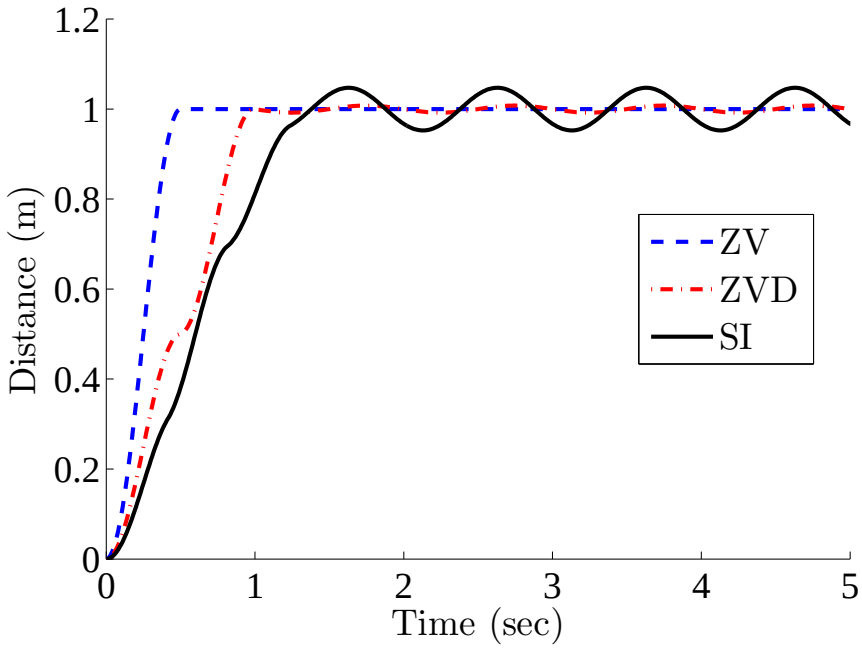

Figure 12: Response of Mass-Spring System to Different Input Shapers

The frequencies ranges are usually determined by finding the modeled frequency and then determining an insensitivity range, I, around that frequency to make the shaper robust to any reasonable modeling errors and parameter variations. The dashed line in Figure 11 represents the tolerable system vibration after input shaping is applied. The insensitivity for this example is 0.67. This is found by dividing the frequency range width by the nominal frequency (1 Hz) in the frequency range.

3.1.5 Application

The SI shaper is a more useful shaper because it allows for the insensitivity to be specified by the designer. The tradeoff for increasing robustness is an increase in rise time of the system. Figure 12 shows an example of the response of a simple mass-spring system with a natural frequency of 1 Hz to different input-shaped step commands. The ZV and ZVD shapers were designed for a 1 Hz system frequency and therefore completely cancel the vibration in the simulation. A robust SI shaper was designed for 1 Hz with an insensitivity of 0.5, and a vibration limit of 5%. When the

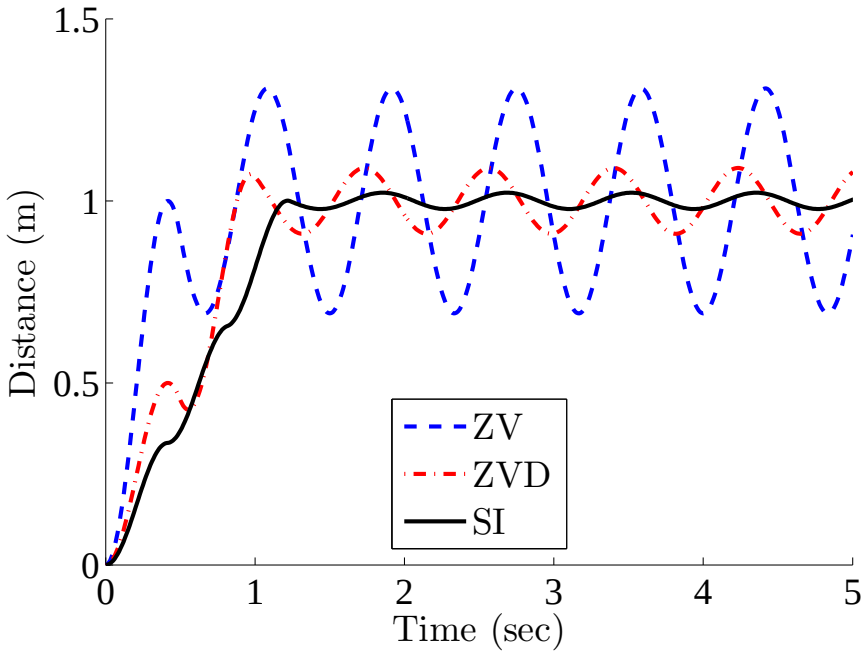

Figure 13: Response of Mass-Spring System With 17% Error in Design Frequencies

design frequency exactly matches the frequency of the system being controlled, the ZV and ZVD shapers exhibit faster rise times and smaller residual vibration because the SI shaper was designed for small amount of residual vibration and a large insensitivity.

Figure 13 shows the strength of the SI shaper, robustness to modeling errors. The design frequency for all shapers is still 1 Hz but now the actual frequency of the system has been changed to 1.2 Hz. As seen in Figure 13, the ZV shaper cannot adequately suppress the vibration of the system. The ZVD does much better than the ZV shaper, but the SI shaper is substantially better than the ZVD shaper. The SI shaper suppresses the vibration down to less than 5% of the step-induced vibration because the system frequency still falls within the insensitivity range. In fact, the frequency would need to increase past 1.25 Hz before the SI shaper would loose its ability to keep the vibration below the tolerance level. Figures 12 and 13 illustrate the trade off between the three shapers, decreased rise time versus increased robustness.

3.2 Two-Mode SI Input Shaping

SI input shaping can be very robust to modeling errors around one frequency. However, many system have more than one significant frequency and thus suppressing only one mode may not be enough to obtain a desirable response. If an SI shaper was designed to suppress two, or more frequencies by using one large frequency suppression range, then the shaper would be very long. It is very easy to extend the concepts presented previously to suppress multiple modes of vibration in a more efficient manner. For the purpose of this chapter, systems with two modes will be considered.

3.2.1 Design

When designing a SI shaper for two modes, the amplitude summation constraint (26), the amplitude positivity constraint (27), and the minimum time constraint (28) are all unaltered. The vibration constraint, (25), is altered to take into account a second mode of vibration:

$$V_{tol} \geq V(\omega_1, \zeta_1) + V(\omega_2, \zeta_2) \tag{29}$$

$V(\omega_1, \zeta_1)$ and $V(\omega_2, \zeta_2)$ are defined as the system vibration caused by each frequency. The constraint now requires that the system vibration at both frequencies, be below some vibration tolerance, V_{tol}. Separating (29) into two equations allows the designer to specify different vibration tolerances for each frequency range, V_{tol1} and V_{tol2}.

$$V_{tol1} \geq V(\omega_1, \zeta_1) \tag{30}$$

$$V_{tol2} \geq V(\omega_2, \zeta_2) \tag{31}$$

Figure 14 shows an example sensitivity curve for an SI shaper suppressing two modes of vibration. Because two frequencies are being suppressed, two distinct frequency ranges need to be used, allowing for the designer to use two insensitivities and two

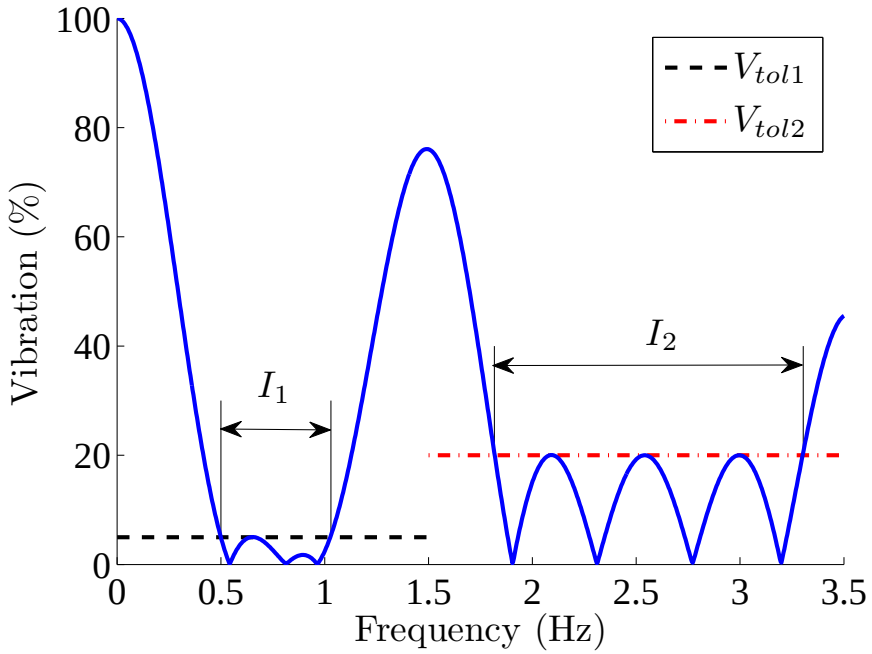

Figure 14: Sensitivity Plot for Two-Mode SI Input Shaper

different vibration limits. This could be useful if the frequency of one mode varies a great deal while the other remains relatively constant, such as in the case of double-pendulum cranes.

3.2.2 Application

Figure 15 illustrates the response of a simple two-mass-two-spring system with frequencies at 0.75 Hz and 2.5 Hz. The ZV or ZVD shapers were created by designing shapers for each of the two modes and then convolving them together to produce the final shaper. The SI shaper was designed using frequency ranges of 0.5 Hz to 1 Hz and 2 Hz to 3 Hz and residual vibration tolerances of 5%. This resulted in an insensitivity of 0.25 for the low frequency and 0.4 for the high frequency. The ZV and ZVD are able to completely remove the vibrations from the response when the design frequencies exactly match the system frequencies. This results in the ZV and ZVD shapers giving a faster system rise time and a lower residual system vibration than the two-mode SI shaper.

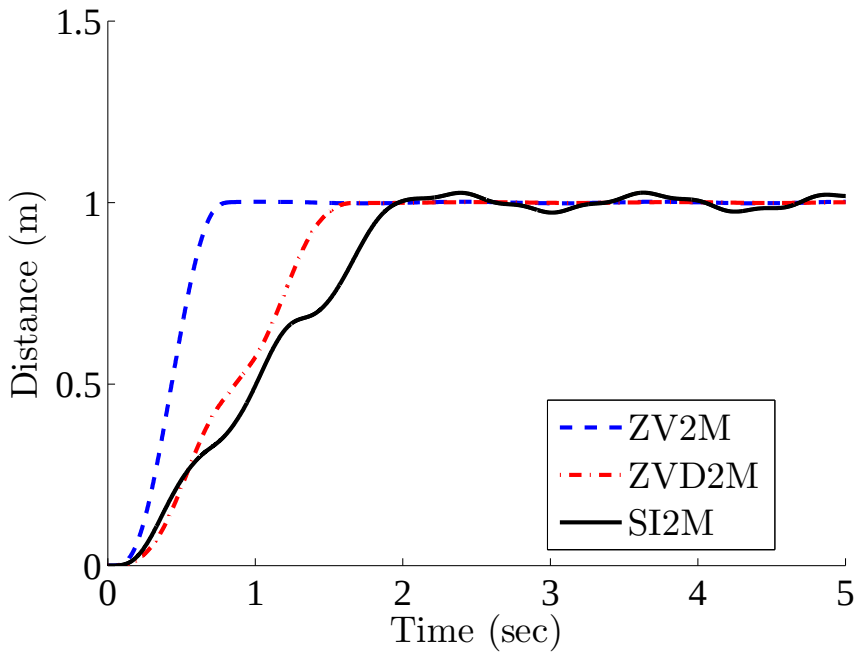

Figure 15: Response of Two-Mass-Two-Spring System to Different Input Shapers

However, Figure 16 illustrates the robustness of the SI shaper to modeling errors in the design frequencies by showing the response when the frequencies are shifted to 0.6 Hz and 2.9 Hz. ZV and ZVD shapers do not suppress the vibration to a tolerable level of 5%. The SI shaper suppresses the vibration of the system to the acceptable vibration level because the system frequencies fall within the insensitivity range of the SI shaper.

3.2.3 Two-Mode SI Input Shaper Algorithm

The following design procedure is the straight forward algorithm for designing the Two-Mode SI Input Shaper [53].

1. Determine frequency ranges to suppress.

2. Set the vibration tolerances for both modes at the desired overall system vibration tolerance level.

3. Solve for the Two-Mode SI input shaper by satisfying the constraint equations while minimizing the shaper duration.

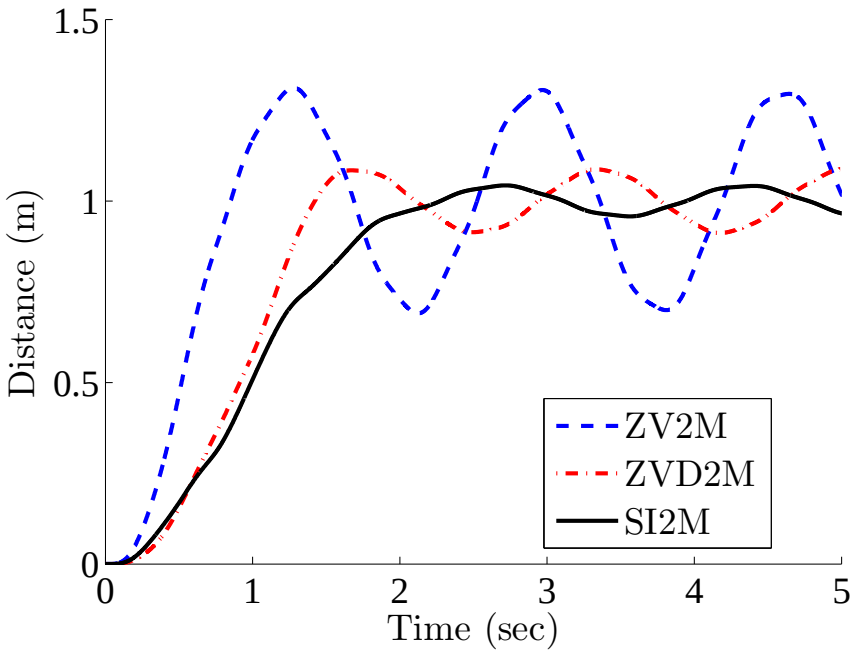

Figure 16: Response of Two-Mass-Spring System With up to 20% Error in Design Frequencies

3.3 Varying Amplitude Contribution Two-Mode SI Shapers

Using SI shapers for two modes of vibration allows the residual system vibration to be reduced to a desired level. The previous section discussed how to accomplish this by setting the vibration tolerances of both modes to the overall desired vibration limit. This approach requires no knowledge of how the frequencies contribute to the overall response of the system. If it is known how the individual frequencies contribute to the overall response of the system vibration, then it is possible to design a more efficient SI input shaper.

3.3.1 Previous Work

Chapter 2 shows that both modes of vibration do not necessarily contribute equally to the overall response of the system. Usually one mode is dominant while the other adds a lesser amount of vibration. Kim and Singhose [55] briefly investigated how

increasing the non-dominant mode vibration tolerance, V_{tol2}, affected the system response for point mass payloads.

The shapers in [55] were designed by varying only the non-dominant mode's vibration tolerance. The dominant mode's vibration tolerance was set to the system's desired vibration tolerance and the second mode's vibration tolerance was relaxed because it does not contribute as much to the system response as the dominant mode. This worked well for many combinations of system parameters, but no algorithm was presented to find a truly optimal shaper. The following sections will outline algorithms for improving two-mode SI shapers based on the ideas and initial work presented previously [55].

3.3.2 Shaper Constraints

Varying Amplitude Contribution Two-Mode SI shapers (VACSI) shapers are developed using knowledge of the amplitude contributions from the system frequencies. The amplitude contributions can be found by developing a model of the system and finding the impulse response of the model, as done in Chapter 2. Alternatively, experimental data from a real machine could be analyzed to obtain the frequency contributions. The VACSI shaper uses (26), (27), and (28) as constraint equations in the same way as the previously presented Two-Mode SI shapers. The vibration tolerance equation, (29), is modified to account for the amplitude contributions of each mode:

$$V_{tol} \geq \alpha_1 V_{tol1} + (1 - \alpha_1) V_{tol2} \tag{32}$$

The VACSI shaper adjusts the vibration tolerance of the non-dominant mode, V_{tol2}, relative to the selected vibration tolerance of the dominant mode, V_{tol1}, using knowledge of the amplitude contributions, $[\alpha_1,\ 1 - \alpha_1]$, of the two modes.

There are two unknowns in (32), V_{tol} and V_{tol1}, that need to be determined before the vibration constraint for the non-dominant mode, V_{tol2}, can be found. The choice

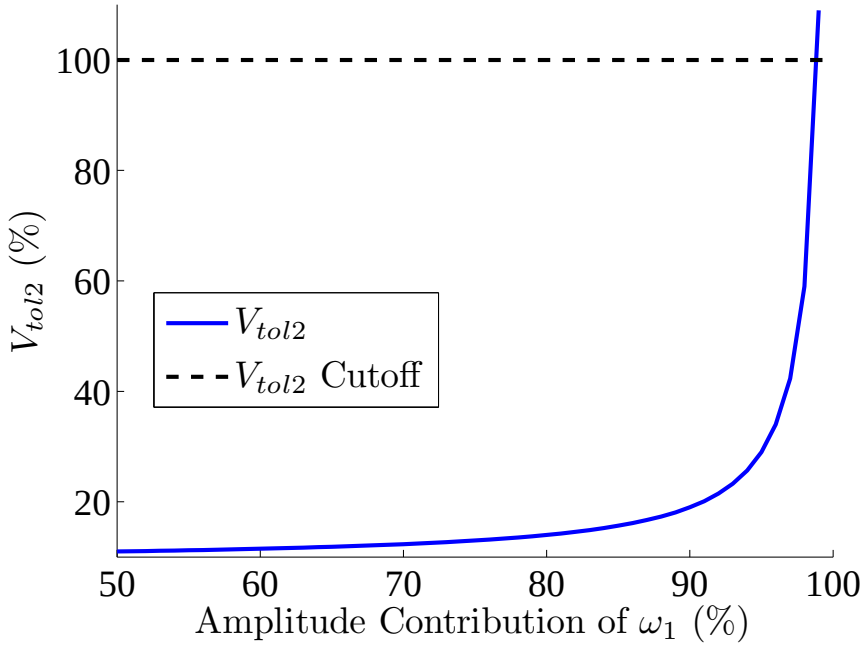

Figure 17: Non-Dominant Mode Vibration Tolerance, V_{tol2}

for the system vibration tolerance, V_{tol}, is dependent on the allowable level of residual vibration in the system; in practice V_{tol} is usually chosen between 5% and 10%. The vibration tolerance of the dominant mode, V_{tol1}, is then chosen at some level below the system vibration tolerance, perhaps 1% - 2% below V_{tol}. The vibration tolerance of the second mode, V_{tol2}, is then calculated by solving (32) for V_{tol2}:

$$V_{tol2} = \frac{V_{tol} - \alpha_1 V_{tol1}}{1 - \alpha_1} \tag{33}$$

The non-dominant mode vibration tolerance, V_{tol2}, found in (33) is used with the chosen dominant mode vibration tolerance, V_{tol1}, to determine the VACSI shaper. Figure 17 shows how the non-dominant mode vibration tolerance changes as the amplitude contribution of the first mode increases. As the amplitude contribution of the first mode approaches 100%, the vibration tolerance of the non-dominant mode increases exponentially. When V_{tol2} increases past 100%, the shaper is no longer designed for two modes. Since it no longer matters how much vibration the non-dominant mode contributes to the system, only a single-mode SI shaper should be used.

3.3.3 VACSI Input Shaping Algorithm

The following design procedure is the algorithm for implementing the VACSI Input Shaper.

1. Determine frequency ranges to suppress.
2. Calculate the Amplitude Contributions of each mode
3. Choose the limitation on the dominant mode, $V_{tol1} < V_{tol}$
4. Calculate V_{tol2} using (33)
5. Determine the Two-Mode SI input shaper by satisfying the constraint equations while minimizing the shaper duration.

3.3.4 Insensitivity

The VACSI shaper is usually shorter than a two-mode SI shaper designed with a straightforward algorithm because it is more intelligently designed. But the VACSI shaper may not be shorter than a two-mode SI shaper. Allowing the amplitude contributions of each mode to modify the vibration tolerances can result is a shaper with a longer shaper duration. This happens when the insensitivity of the dominant mode is larger than the non-dominant mode.

Figure 18 shows a comparison between the shaper duration of VACSI shapers and standard SI shapers designed for frequencies of 0.25 Hz and 0.6 Hz. The insensitivity of the dominant mode, I_1, was set to 0.06, 0.12, and 0.18, while the insensitivity of the non-dominant mode, I_2, was held constant at 0.12. The horizontal dashed lines represent the time duration of the SI shapers designed for the three specific insensitivities. Figure 18 shows that as I_1 increases, the shaper duration increases. When I_1 becomes greater than I_2 (0.12), the shaper duration of the VACSI shaper is no longer shorter than the duration of the standard SI shaper. Figure 19 shows shaper duration when I_1 is increased up to 0.6 (I_2 is once again set to 0.12).

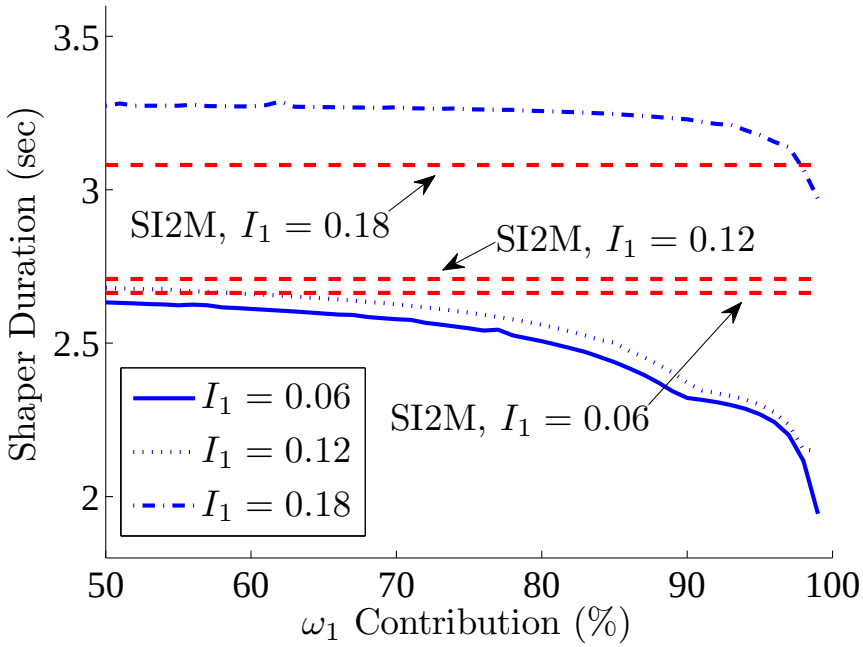

Figure 18: VACSI Shaper Duration for Various ω_1 Insensitivities

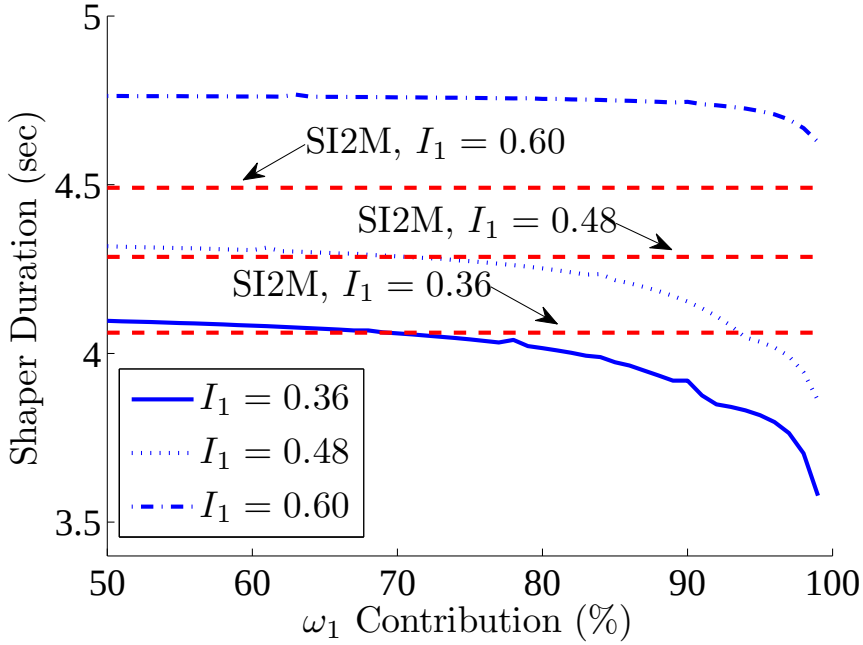

Figure 19: VACSI Shaper Duration for Various Higher ω_1 Insensitivities

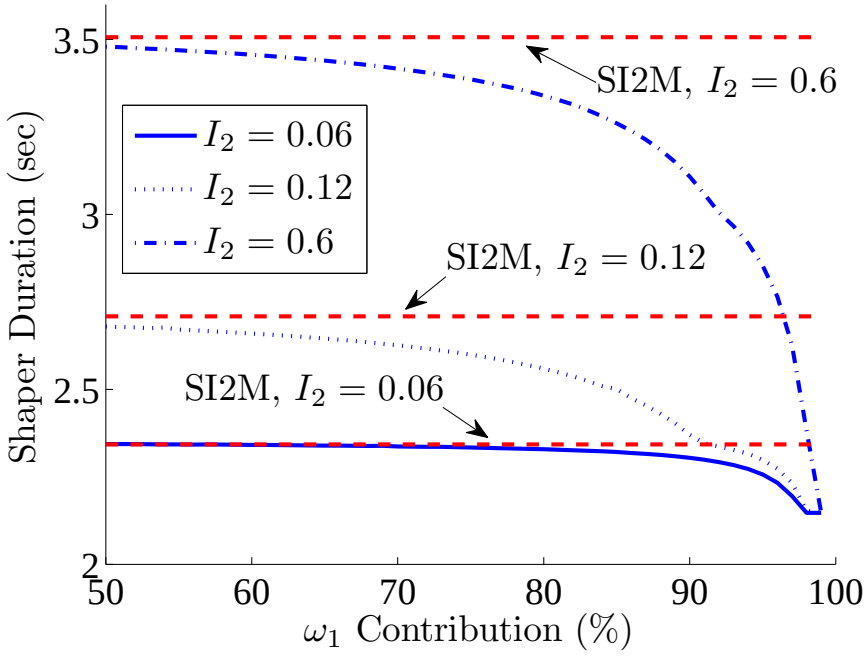

Figure 20: VACSI Shaper Duration for Various ω_2 Insensitivities

Figure 19 shows that the shaper duration will no longer stay below the duration of the standard SI shaper once the insensitivity of the dominant mode is increased beyond that of the non-dominant mode. Where they cross the SI2M line is a function of sensitivity curves. In many systems, the dominant mode frequency is known with more certainty than the non-dominant mode frequencies. This may allow for the insensitivity requirement of the dominant mode to be smaller. This leads to the need for a larger non-dominant mode frequency insensitivity when designing a shaper for two modes.

Figure 20 shows the shaper duration of VACSI shapers versus the duration of standard SI shapers for various non-dominant mode insensitivities, I_2. The dominant mode insensitivity, I_1, is set at 0.12. From this figure, it can be seen that for even large non-dominant mode insensitivities, the shaper duration of the VACSI shaper still remains at or below the shaper duration of the standard SI shapers. When the insensitivity is small, the shaper duration advantage of the VACSI shaper is not large and does not become evident until the amplitude contribution of the dominant mode

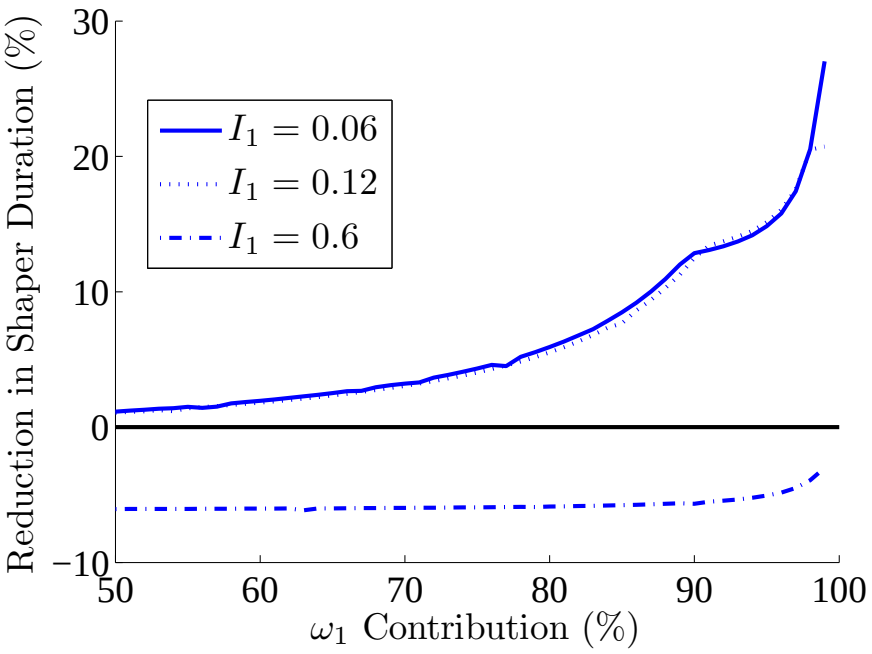

Figure 21: Reduction in Shaper Duration for Various ω_1 Insensitivities

is above 80%. However, at large values of low-mode contribution, this new design method produces substantially faster two-mode SI shapers. At higher insensitivities, the decrease in shaper duration is evident over most of the range of dominant mode amplitude contributions.

3.3.5 Shaper Duration

The previous section showed that the design insensitivities greatly affected the duration of the VACSI shaper. Therefore, it is important to clearly understand the potential advantage of the VACSI shaper. Figure 21 shows the percentage reduction in shaper duration when using a VACSI shaper versus a two-mode SI shaper when the insensitivity of the non-dominant mode is set to 0.12.

This figure shows that when the required insensitivity of the dominant mode becomes larger than the insensitivity of the non-dominant mode, the shaper no longer provides a shorter shaper duration. Because many systems require a larger insensitivity in the non-dominant mode than the dominant mode, such as the crane modeled

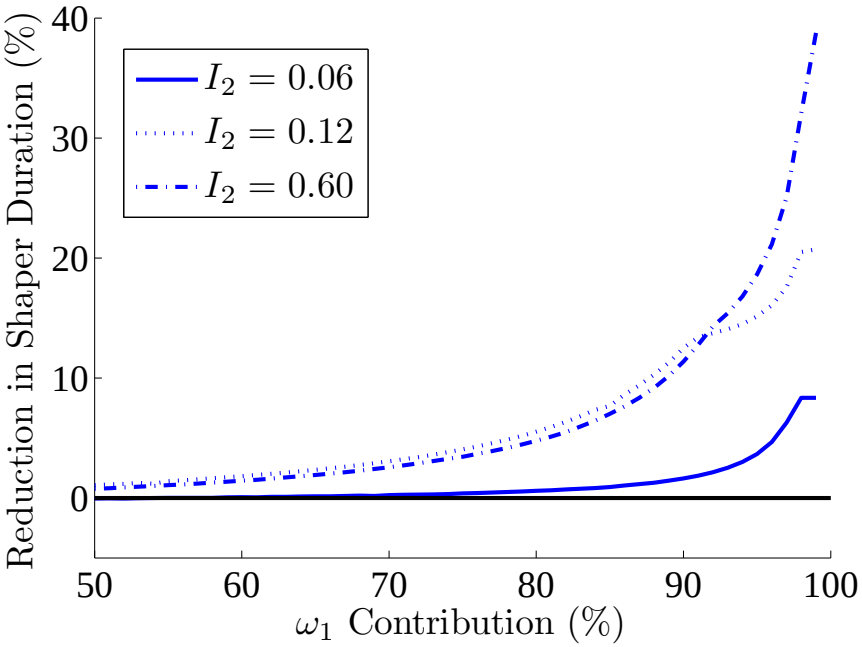

Figure 22: Reduction in Shaper Duration for Various ω_2 Insensitivities

in Chapter 2, this is acceptable.

The percentage reduction in shaper duration when using a VACSI shaper versus a standard SI shaper as a function of the non-dominant mode insensitivity is shown in Figure 22. The insensitivity of the dominant mode held constant at 0.12.

In Figure 22, the non-dominant mode insensitivity, I_2, does not cause the VACSI shaper to become longer in duration than the standard SI shaper. When I_2 in smaller than I_1 the amplitude contribution from the first mode must be large, approximately 80%, for the VACSI shaper to have an advantage over the standard SI shaper. As I_2 increases, the advantage of the VACSI shaper is noticeable over more of the range of dominant mode amplitude contributions.

3.3.6 Simulation Verification

A crane simulation was used to verify that the VACSI shaper produces a response that meets design requirements and is faster than a two-mode SI shaper. The simulated crane is the same as analyzed in Chapter 2. The parameters used in the simulation

Table 3: Crane Simulation Parameters

Suspension Cable Length	3.0 m
Rigging Length	3.0 m
Payload Mass	50 kg
Hook Mass	75 kg
Payload Radius of Gyration	3.0 m
Move Distance	1.7 m

are tabulated in Table 3.

Given the values in Table 3, the two frequencies are $\omega_1 = 0.19$Hz and $\omega_2 = 0.35$Hz. The amplitude contributions of each mode were calculated from the impulse response to be, $\alpha_1 = 0.89$ and $(1 - \alpha_1) = 0.11$. To accommodate uncertainty in the determination of the frequencies, the insensitivities of the VACSI shaper were set to $I_1 = 0.1$, and $I_2 = 0.26$. A vibration tolerance for the system was chosen at 0.1 (10%). The vibration tolerance for the dominant mode was set at 0.09 (9%). Using (33), the vibration tolerance of the non-dominant mode, V_{tol2}, was calculated to be 0.18 (18%). Using this information, the VACSI shaper was calculated to be:

$$\begin{bmatrix} A_i \\ t_i \end{bmatrix} = \begin{bmatrix} 0.26 & 0.24 & 0.24 & 0.26 \\ 0 & 1.4 & 2.5 & 3.9 \end{bmatrix} \tag{34}$$

Figure 23 shows the sensitivity curve for the VACSI shaper designed for this scenario.

Figure 24 shows response of the system when the overhead trolley is moved 1.7 m. The frequencies of the system line up exactly with the design frequencies for the VACSI shaper.

The residual vibration in the system after the shaped move is 5% of the unshaped case. This is half the maximum allowable residual vibration for the system. By using the VACSI shaper, the rise time is 11%, or 0.5 seconds, shorter than a standard two-mode SI shaper. An 11% reduction in rise time can be significant to operating

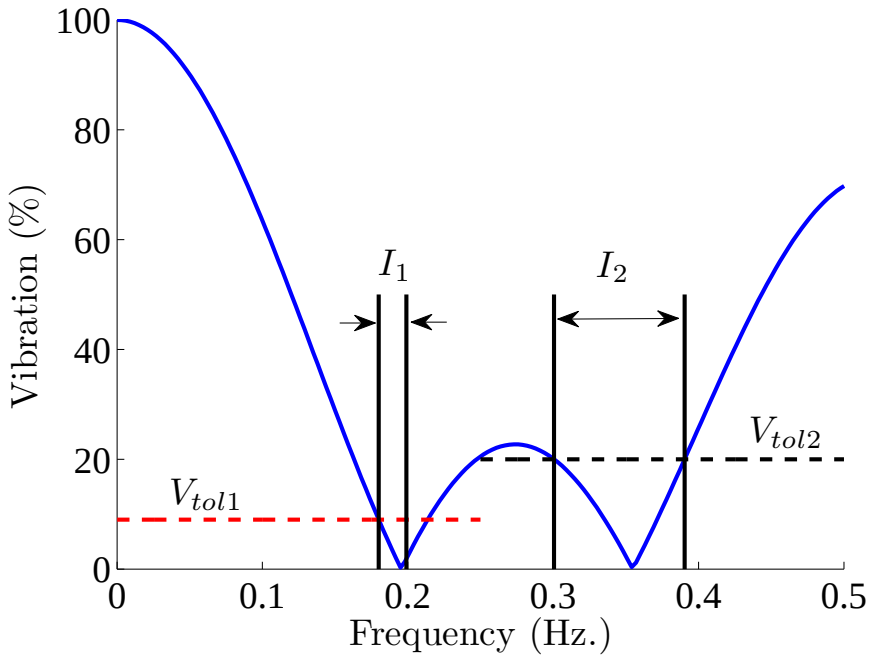

Figure 23: Simulation VACSI Shaper Sensitivity Curve

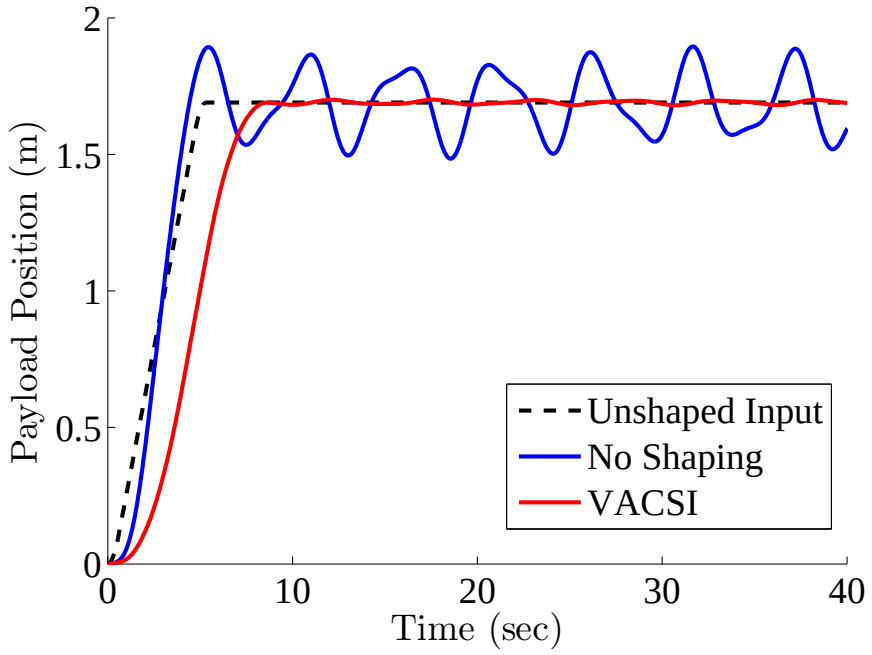

Figure 24: Simulated Crane Response

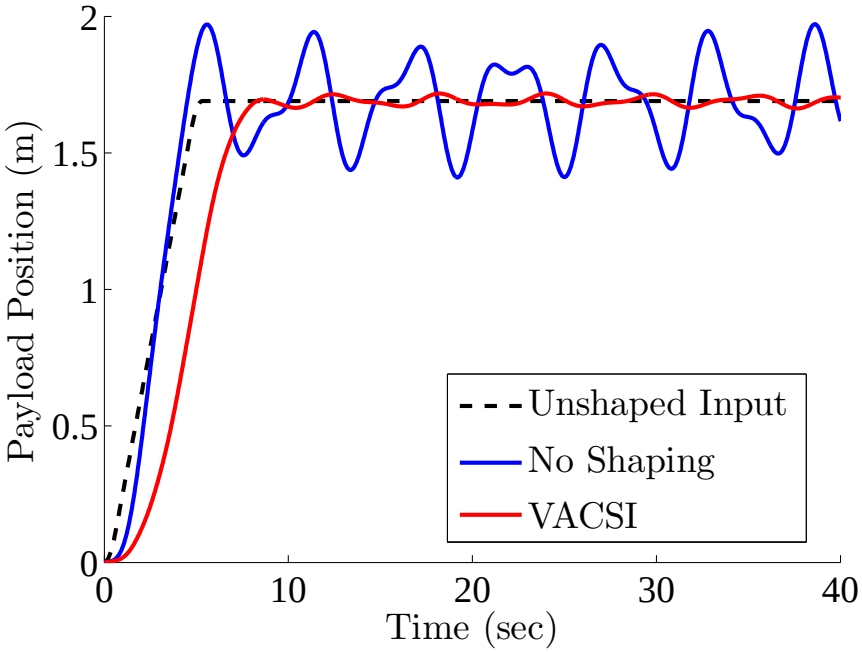

Figure 25: Simulated Crane Response with Inaccurate Model Frequencies

efficiency. For industrial machinery such as cranes, this time reduction translates directly into increased throughput.

Figure 25 shows the payload response when the payload's radius of gyration is actually 3.4 m rather than 3.0 m. This parameter change causes the system frequencies to shift to $\omega_1 = 0.18$ and $\omega_2 = 0.33$. The dominant mode frequency, ω_1, is now at the edge of the shaper insensitivity. From Figure 25, it can be seen that even with radius of gyration being off by 12%, the residual vibration of the response with the VACSI shaper is still 10%.

3.3.7 Vibration Tolerances

3.3.7.1 Increasing V_{tol2}

When designing the VACSI shaper, the vibration tolerance of the non-dominant mode, V_{tol2} is determined by (33). This results in a shaper that satisfies all the design requirements for the system and, in many cases, results in a faster shaper than a standard two-mode SI shaper. In some cases, it is possible to set V_{tol2} higher than the

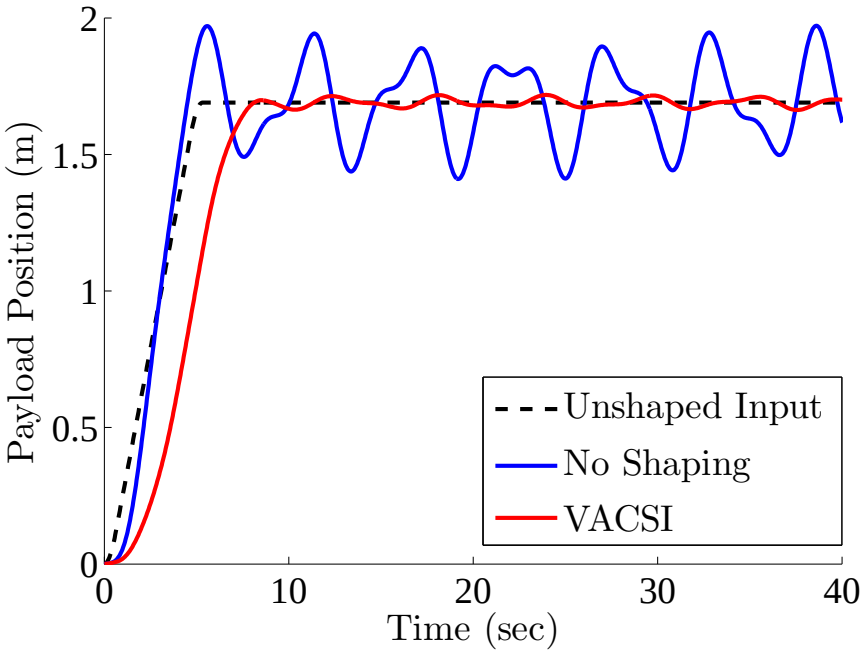

Figure 26: Response with Inaccurate Model Frequencies and $V_{tol2} = 0.2$

result given in (33). To do this, a simulation of the system is required. This enables the designer to modify the V_{tol2} value and check that the response of the system is still acceptable.

Figure 26 shows the response of the same system used in the previous section when V_{tol2} is increased from 0.18 to 0.20. The time duration reduction for the shaper increases to 15% and the residual system vibration remains at 10%. If V_{tol2} is raised to 0.25, the time reduction increases to 18% and the residual vibration in the system increases to 12%, which in many industrial applications may still be acceptable.

To gain the additional shaper duration reduction, the following additional steps need to be done after the VACSI shaper is found.

1. Increase V_{tol2} by Y%

2. Solve the Two-Mode SI input shaper using the new value in the constraint equations

3. Check the residual system vibration by running a simulation for many combinations of the two modes

4. Repeat steps 2 and 3 until the response of the simulation no longer meets the residual vibration requirement

3.3.7.2 Decreasing V_{tol1}

Reducing the vibration tolerance of the dominant mode allows for a larger increase in the non-dominant vibration tolerance. Continuing to decrease V_{tol1} will eventually cause the VACSI shaper duration to become longer than a standard two-mode SI shaper designed at the system vibration tolerance. This crossover point is a product of the way in which the sensitivity curves for the two modes interact. Linearized simulations should be used to verify that the VACSI shaper still meets the design requirements.

3.4 Summary

Two-mode SI shapers are designed by obtaining the expected frequency ranges of the system and calculating the shaper using a vibration tolerance limit. The SI shaper is designed using (25) or (29), (26), (27), and (28). To decrease the shaper duration of the system, a VACSI shaper can be employed by finding the amplitude contributions of each mode and modifying the vibration tolerance of the non-dominant mode using (33). The insensitivity of the dominant mode determines if the VACSI shaper will give a shorter shaper than a two-mode SI shaper. When the insensitivity of the dominant mode is larger than the non-dominant mode insensitivity, the VACSI shaper may not improve the shaper duration. The non-dominant mode insensitivity changes the amount by which the shaper duration will decrease, but it will still decrease. Simulations of a crane show that a VACSI shaper can provide more than a 10% decrease in the shaper duration, while the residual vibration of the response remains

below the tolerable level.

CHAPTER IV

EXPERIMENTS ON FLEXIBLE SYSTEMS

In Chapter 3, a new algorithm for optimizing the constraint equations for a two-mode SI shaper was presented and simulations verified the new algorithm. This chapter will present experimental verification of this VACSI algorithm on a 10-ton industrial bridge crane and a long-reach robotic arm (RALF) with two-links.

4.1 Robotic Arm Long and Flexible (RALF)

As discussed in Chapter 1, flexible robotic arms in industry are challenging to use because it is difficult to position the end-effector of the robot accurately and without vibration. In the experiments reported in this chapter, a feedback controller in conjunction with a VACSI input shaper was used to move the endpoint of RALF with very little vibration.

4.1.1 Experimental Setup

RALF is sketched in Figure 27 [8, 31, 38]. RALF consists of two 2.54 m hollow aluminum links which are actuated by two hydraulic cylinders attached to the base of the robot. The second link is attached to a hydraulic cylinder by an actuation link. The angles of each link, θ_1 and θ_2, are calculated from the extension lengths of the hydraulic actuators.

To control the position of RALF, a position feedback controller was designed for each link. The controller used for this system was designed in Simulink using the XPC-Target toolbox. A diagram of the controller for Joint 1 is shown in Figure 28. The tip position was recorded using a Sony camcorder running at 30 fps. The camera tracked a small circle on a white background attached to the end of link 2.

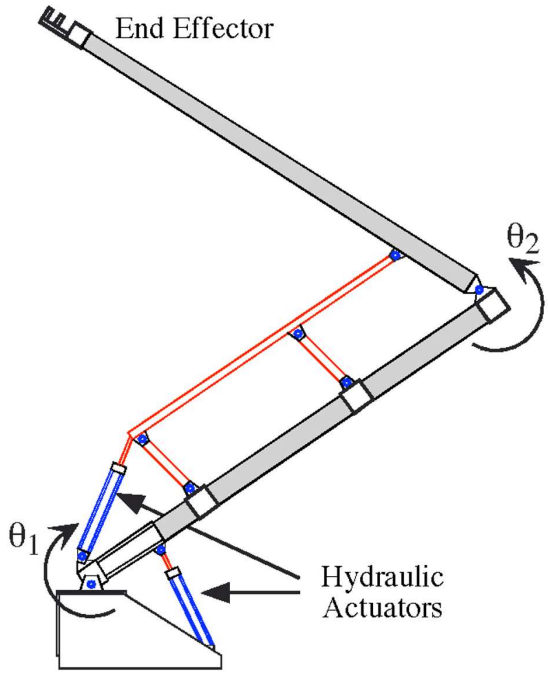

Figure 27: Diagram of RALF

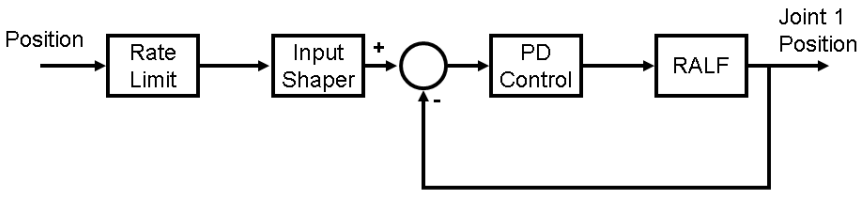

Figure 28: RALF: Joint 1 Controller

The input for Joint 1 was given as an angle that was converted into a cylinder shaft position corresponding to a desired configuration of RALF. The signal was then rate limited to avoid saturating the hydraulics. Then, the signal was shaped to reduce the induced vibration. A proportional-derivative (PD) feedback controller was designed to move the system faster and remove some of the vibration through derivative control action. Joint 1 was operated around $\theta_1 = 140\,\text{deg}$. The range of motion for this experimental setup was confined to actuation of θ_1, therefore, only a proportional controller was used on joint 2. This was possible because the hydraulic cylinders are very stiff and could not be displaced by the vibrations once positioned.

RALF has two dominant flexible modes. To find the frequency and amplitude contributions of each mode, the tip of RALF was deflected and released and the tip response was recorded. The frequencies were found using an FFT of the response. The amplitude contribution of each mode were found by canceling the response with sine waves at each frequency. The frequencies of RALF are shown in Figure 29. The dominant mode of the system was the low mode at approximately 89% of the total response. When a 5 lb weight was attached to the tip of the robot, the frequencies dropped by about 0.4 Hz and the amplitude contribution of the dominant mode stayed roughly the same around the operating point of the robot.

A two-mode SI shaper, and a VACSI shaper were designed for the amplitude contribution of 89% and frequency suppression ranges of 3.8 to 4.3 Hz and 4.6 Hz to 5.4 Hz:

$$\begin{bmatrix} A_i \\ t_i \end{bmatrix} = \begin{bmatrix} 0.26 & 0.48 & 0.26 \\ 0 & 0.11 & 0.21 \end{bmatrix} \quad \text{(Two-Mode SI)} \tag{35}$$

$$\begin{bmatrix} A_i \\ t_i \end{bmatrix} = \begin{bmatrix} 0.26 & 0.48 & 0.26 \\ 0 & 0.10 & 0.19 \end{bmatrix} \quad \text{(VACSI)} \tag{36}$$

Both shapers were designed using a residual system vibration tolerance of $V_{tol} = 5\%$. The two-mode SI shaper (35) was designed using $V_{tol1} = V_{tol2} = 5\%$. The VACSI

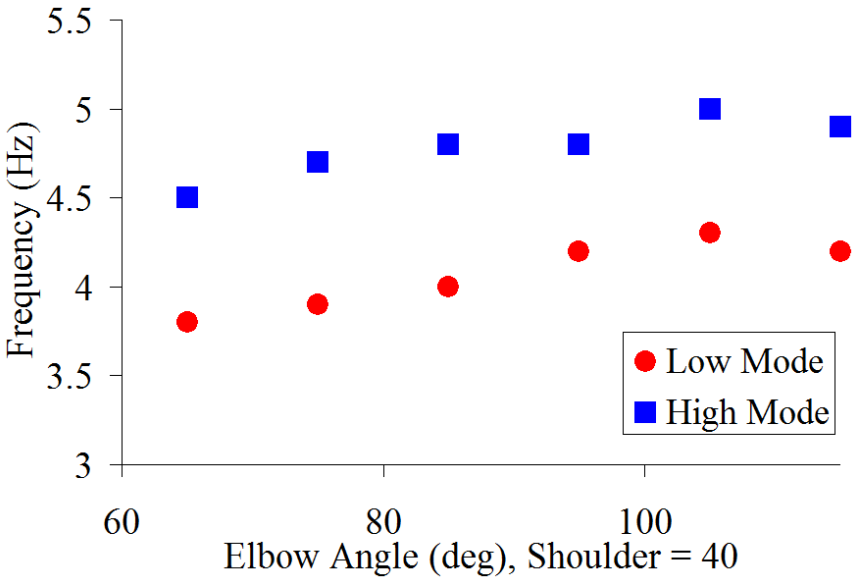

Figure 29: Frequencies of RALF

shaper (36) used a $V_{tol1} = 4\%$ and (33) to find $V_{tol2} = 14\%$. As can be seen from (35) and (36), the VACSI shaper is 9.5% faster than the two-mode SI shaper.

4.1.2 Experimental Results

Joint 1 was moved from 40° to 50° while joint 2 was held constant at 75°. The response of the tip is shown in Figure 30. The figure shows the tip position response when moved using no shaper, the SI2M shaper, and a VACSI shaper. It can be seen from the figure that the SI2M shaper and the VACSI shaper induces very little vibration in the tip. Two-mode SI shaping suppressed the vibration in the system to the desired level, but it required a slower rise time. A VACSI shaper has the same effectiveness as a two-mode SI shaper and was 9.5% faster, allowing for a faster response with the same accuracy. The results were similar when the 5 lb weight was attached to the tip of the robot.

4.2 10-ton Industrial Bridge Crane

The 10-ton bridge crane at Georgia Tech is used in a variety of applications ranging from moving supply pallets to servicing machinery. Because the work area where the

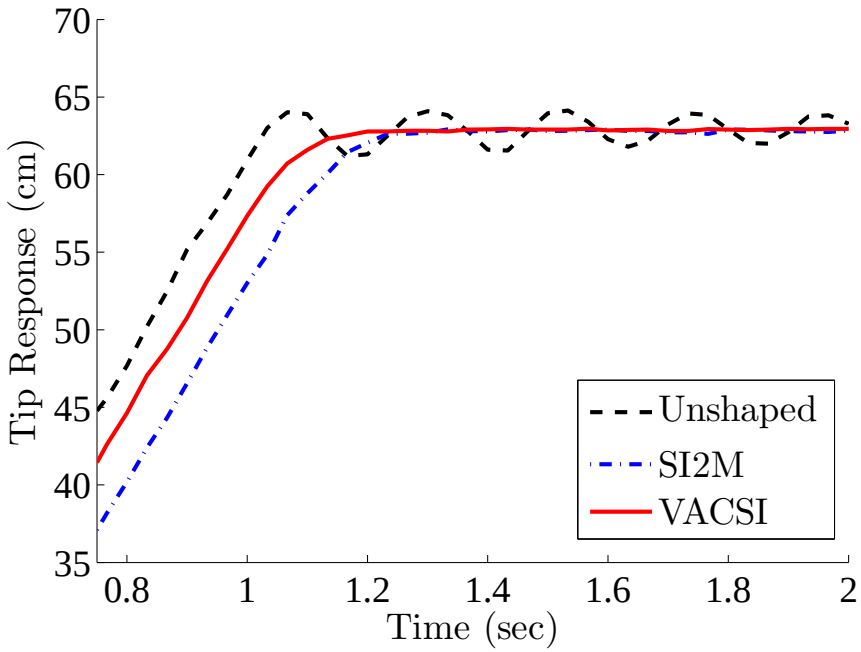

Figure 30: RALF Tip Position Response

crane resides is crowded, it is important to have precise control of the payload to avoid damaging other machinery and endangering people.

4.2.1 Experimental Setup

The bridge crane is run using an open loop controller in the velocity domain. When input shaping is enabled, the input to the controller is a velocity profile that is shaped and rate limited before being sent to the motor drives. The crane setup is seen in Figure 31. The hook mass was approximately 50 kg and the payload mass was approximately 53 kg. The payload ranges in a radius of gyration of 0.29 m to 0.82 m. The payload is a rectangular box with pins along the center axes to attach weights. By arranging the weights in different configurations, the payload's radius of gyration can be set to different values[1]. The payload position was measured using a Siemens camera tracking system. A more in-depth discussion of the crane setup is found in Chapter 5.

[1]The payload was built with great assistance by Jeffrey Clement

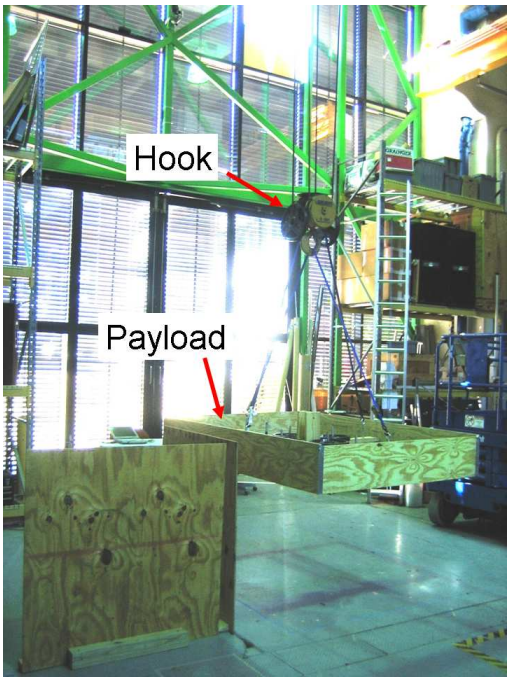

Figure 31: Crane for VACSI Experiments

The shapers for this experiment were designed using the dynamic analysis found in Chapter 2. The radius of gyration of the payload used for the experiment in this section was 0.73 m and the mass of the payload was 53 kg. The frequencies were found using (14) and (15). The dominant frequency is 0.23 Hz with an amplitude contribution (23) of 95%. The non-dominant mode frequency is 0.53 Hz with an amplitude contribution of 5%. A two-mode SI shaper and a VACSI shaper were both designed for insensitivities of $I_1 = 0.1$ and $I_2 = 0.2$. The residual vibration tolerance for the system was set at 10%. The SI shaper set $V_{tol1} = V_{tol2} = 10\%$. The VACSI shaper set $V_{tol1} = 9\%$, and using (33), set $V_{tol2} = 28\%$. This resulted in:

$$\begin{bmatrix} A_i \\ t_i \end{bmatrix} = \begin{bmatrix} 0.26 & 0.24 & 0.24 & 0.26 \\ 0 & 0.88 & 2.15 & 3.04 \end{bmatrix} \quad \text{(Two-Mode SI)} \tag{37}$$

$$\begin{bmatrix} A_i \\ t_i \end{bmatrix} = \begin{bmatrix} 0.43 & 0.15 & 0.43 \\ 0 & 1.23 & 2.46 \end{bmatrix} \quad \text{(VACSI)} \tag{38}$$

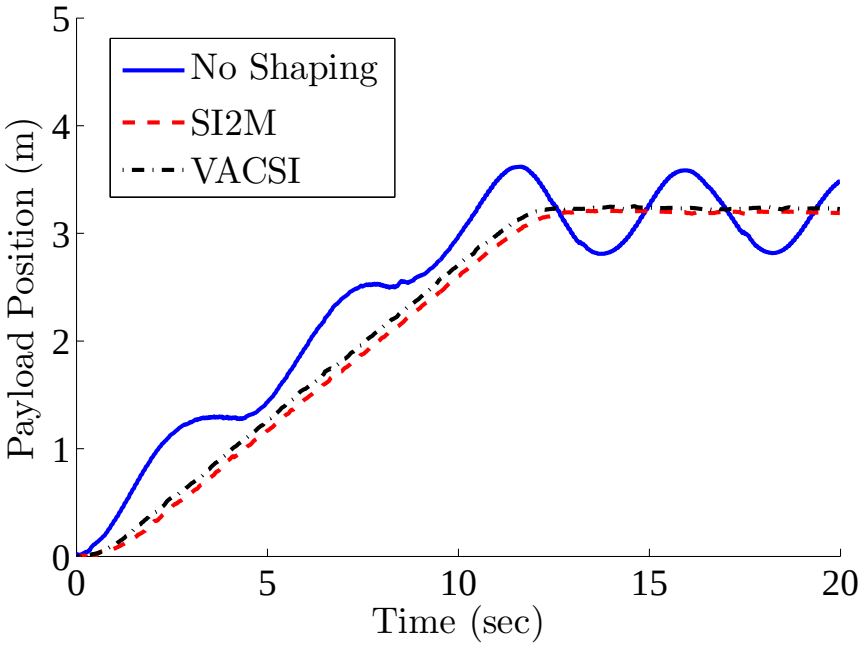

Figure 32: Crane: Payload Position Response

Comparing (37) and (38), it can be seen that the VACSI shaper is 19% faster than the two-mode SI shaper.

4.2.2 Experimental Results

Figure 32 shows the response of the payload to an unshaped command, a two-mode SI shaped command, and a VACSI shaped command. From the figure, it can be seen that the shaped commands suppress both frequencies very well. The two-mode SI shaped response has a residual vibration of 5% and the VACSI shaped response has a residual vibration of 4%. Both shapers suppress the residual vibration to well below the tolerance level of 10%.

4.3 Conclusions

Experiments with a two-link robot, RALF, and the 10-ton industrial bridge crane showed the VACSI shaper to be faster than the two-mode SI shaper and able to suppress the residual tip vibration. The frequencies and amplitude contributions for the RALF experiment were found using an experimental method using ZV shapers

to extract the frequencies and amplitude contributions. These results confirm the analysis presented in the previous chapter.

CHAPTER V

OPERATOR STUDIES

A large body of literature has addressed the benefits of input shaping on cranes [15, 19, 23, 24, 25, 28, 56, 62, 67]. Some of the most valuable validation of input shaping comes when human operators are part of the control loop. This allows the controller to be subjected to a highly diverse set of tests because operators have unique techniques for handling crane operation. Khalid et. al. studied operator performance on single-pendulum cranes using input shaping in [25]. Kim et. al. investigated human operator control of cranes using input shaping in with double pendulum cranes moving point masses around and over obstacles. This research demonstrated that Two-Mode SI input shaping significantly improves performance for both novice and experienced operators. This research was extended to mobile tower cranes by Vaughan et. al. Operators moved a payload using input shaping and also conducted tests via tele-operation of the mobile tower crane from a remote location.

Prior investigation has demonstrated that input shaping works well on systems that can be modeled using point-mass payloads. But the degree of effectiveness on cranes with distributed payloads remains an open question. This chapter will investigate the case when human operators move distributed payloads around and over obstacles. Two studies are presented. The objective of the first study was to understand how different input-shaping techniques help with moving distributed payloads. The second study investigated the learning ability of novice crane operators both with and without input shaping.

5.1 Distributed Payload Crane Operator Study

Input shaping was demonstrated to decrease the vibration of the systems described in Chapters 3 and 4. In the laboratory, with predefined moves executed by computers, it is easy to see the merits of many types of control systems. However, it is also easy to miss possible drawbacks of a controller. Studying the controller in industrial settings in conjunction with human operators allows for a more diverse and thorough investigation of the controller. This evaluation leads to a more in-depth understanding of the controller strengths and weaknesses.

This operator study investigates use of a crane carrying a distributed payload. Two tasks were performed by the operator using three different control techniques. Task 1 was to move a payload around an obstacle. In Task 2 the operators moved a payload over the obstacle. The three control techniques evaluated were: No Input Shaping, Two-Mode ZV Input Shaping, and Two-Mode SI Input Shaping.

5.1.1 Experimental Setup

Figure 33 shows the bridge crane used in the study with the long, distributed payload attached. The payload was initially suspended 18 cm off the ground. For Task 1, the operator was not allowed to changed the height of the payload. For Task 2, the operator hoisted the payload over the obstacle. The task was considered finished when the payload returned to approximately 18 cm off the ground and the payload remained within the circular target area. These two tasks were conducted to study different variables introduced by different types of motion. Moving around the obstacle was used to study the effects of two-dimensional motion. The hoisting task caused the frequencies of the system to change, allowing for the study of the robustness of the shapers to time-varying frequencies [56]. The study was conducted using the test course shown in Figures 34 and 35. The goal was to drive the payload from the 0.5 m sided square to the 0.75 m diameter circle. The operator was required to position

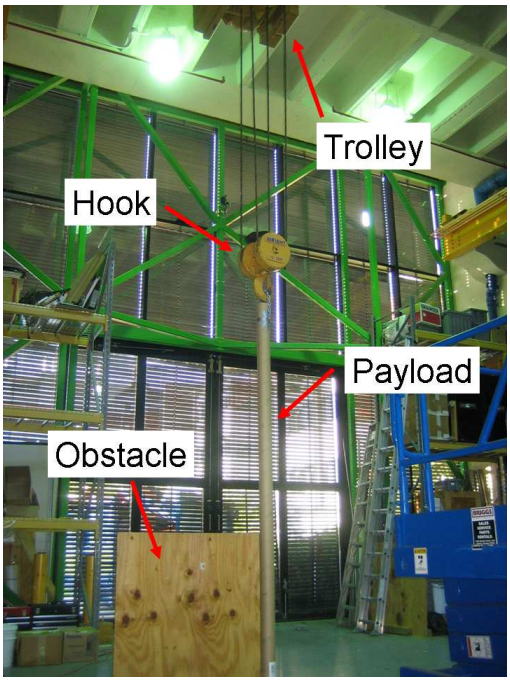

Figure 33: Picture of Industrial Bridge Crane at Georgia Tech

the payload within the target zone with the payload not oscillating out of the zone.

The payload used in this study was a packing cylinder carrying sand. The cylinder is 2.5 m tall with a diameter of 18 cm. The cylinder, seen in Figure 36 was suspended from the crane hook using a steel chain wrapped around the hook and secured to the cylinder through holes drilled into the sides. The chain loop was kept as short as possible to reduce its effect on the system dynamics. The cylinder weighed 22 kg. The hook was modeled as a point mass. The weight of the hook was approximately 50 kg.

The height of the bridge crane from the trolley to the floor was 6.2 m. The initial suspension length was 3.5 m. The crane had an acceleration limit of 0.572 $\frac{m}{s^2}$ and a velocity limit of 0.358 $\frac{m}{s}$. The operator interface for the study was a standard crane pendent, shown in Figure 37, with six directional buttons that allowed the user to move the crane at half speed or full speed.

The time for task completion, hook movement, and operator effort were recorded. The time to completion was measured from when the operator first pushed a button

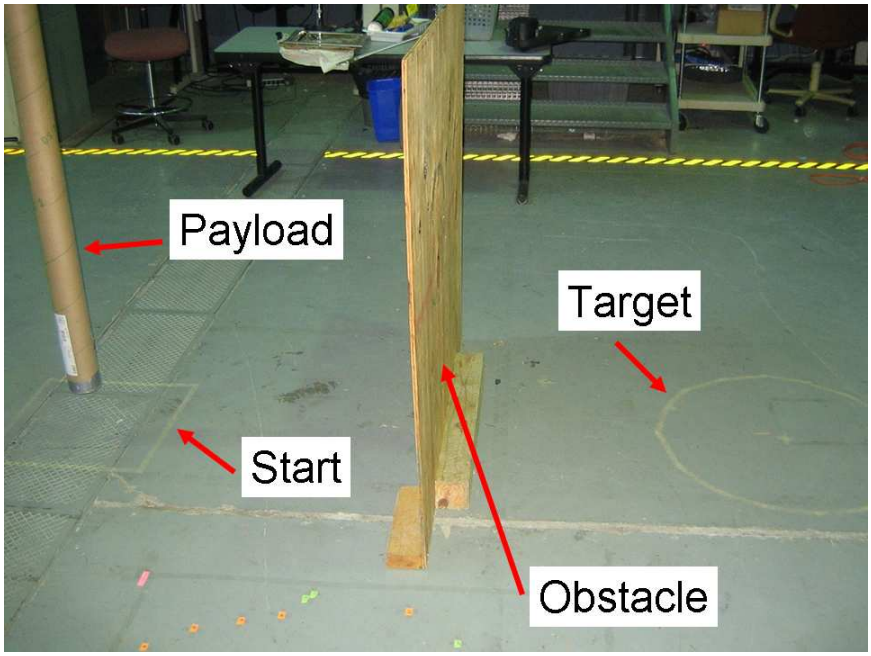

Figure 34: Picture of Operator Study Test Course

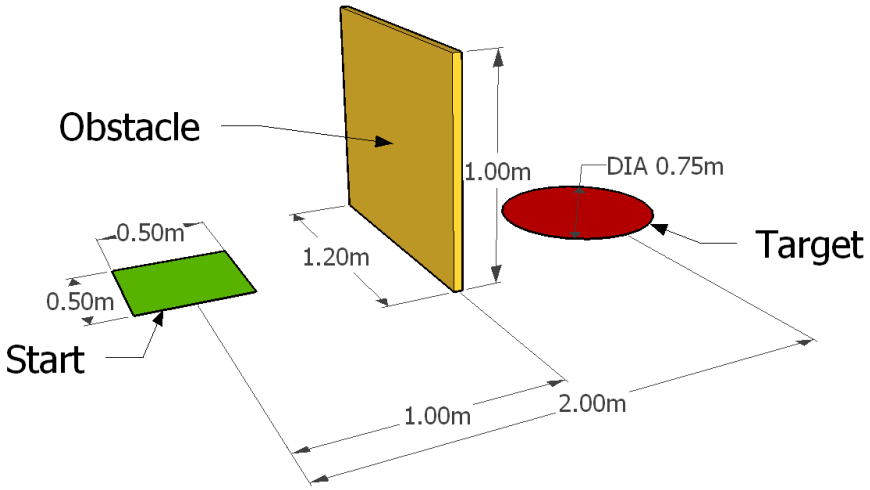

Figure 35: Diagram of Operator Study Test Course

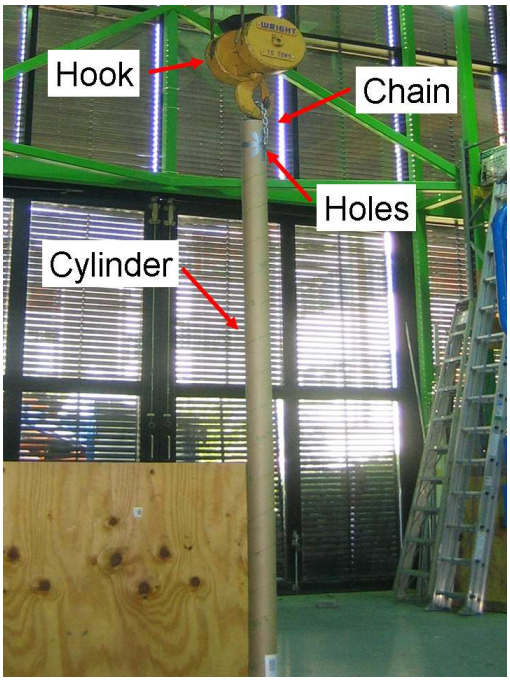

Figure 36: Picture of Cylinder Payload

Figure 37: Picture of Crane pendent

on the crane pendent until the payload remained within the target zone. The hook movement data was collected using a Siemens VS723-2 machine vision system attached to the trolley and a Banner LT3 Time-of-Flight laser positioning system along the crane bridge and support rails. The payload movement could not be directly measured because the camera view is blocked by the suspension cables and the hook. Furthermore, no practical sensor system could be attached to the crane payload. However, the hook movement gives a good estimate of final position and dynamic response of the system throughout the move. The operator effort was measured as the number of times the operator pushed the buttons on the pendent to move in the horizontal directions.

The study was conducted using 17 graduates students enrolled in an advanced controls course at Georgia Tech [60]. Each operator required approximately 35-40 minutes to complete the study. The operators were given 10 minutes to familiarize themselves with the pendent and operation of the crane with the payload. During this time, the operator was able to drive the crane around with and without input shaping. Each operator completed a total of six trials, three moving around the obstacle, and three hoisting over the obstacle. The order of tasks was randomized to avoid operator learning influencing the results.

5.1.2 Shaper Design

Two shapers were developed for the study, a Two-Mode ZV Shaper and a Two-Mode SI Shaper. The ZV shaper was designed using the two dominant frequencies exhibited by the system when the cylinder was suspended 18 cm off the ground. The SI shaper was designed for the two dominant frequency ranges found when suspending the payload 18 cm off the floor and 1.2 m off the floor, the height required to clear the obstacle. The shaper was designed using the standard SI input shaper method reviewed in Chapter 3. The constraint on the residual vibration amplitude was set to

Table 4: Operator Study Design Frequencies

Height off Floor	Low Frequency	High Frequency
18 cm	0.25 Hz	0.44 Hz
1.2 m	0.29 Hz	0.48 Hz

5% for the design of the SI input shaper. The reason for this value selection is that the crane is run without a feedback control loop. This means that the shaper must do all the vibration suppression without the aid of a feedback control loop to aid it. This setup is typical of most cranes used in industry.

The design frequencies were predicted using the frequency equations for distributed payload cranes found in Chapter 2. To verify the theoretical predictions, the experimental frequencies were found by pushing the suspended payload and recording the swing angle of the hook. The recorded data was analyzed using a fast fourier transform to extract the two dominant frequencies of the system. The predicted frequencies were very close to the experimental frequencies. The design frequencies can be seen in Table 4.

The Two-Mode ZV shaper used the design frequencies at a payload height of 18 cm above the floor. This resulted in:

$$\begin{bmatrix} A_i \\ t_i \end{bmatrix} = \begin{bmatrix} 0.25 & 0.25 & 0.25 & 0.25 \\ 0 & 1.26 & 1.99 & 3.12 \end{bmatrix} \quad \text{(Two-Mode ZV)} \tag{39}$$

Two ZV shapers were designed for each of the estimated frequency modes and then convolved together to create the Two-Mode ZV shaper.

The measured frequencies in Table 4 have some uncertainty, therefore the SI shaper was designed using frequency ranges ±5% wider than the design frequency ranges. The SI shaper designed for these design parameters is:

$$\begin{bmatrix} A_i \\ t_i \end{bmatrix} = \begin{bmatrix} 0.16 & 0.34 & 0.34 & 0.16 \\ 0 & 1.35 & 2.68 & 4.01 \end{bmatrix} \quad \text{(Two-Mode SI)} \tag{40}$$

Figure 38 shows the sensitivity curves for the two shapers.

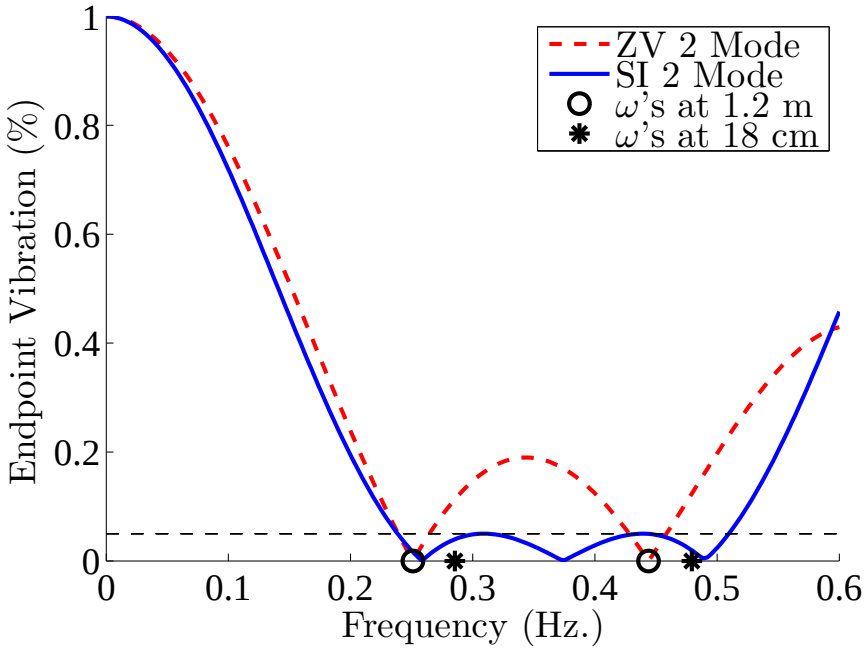

Figure 38: Sensitivity Curves for Operator Study Shapers

Examining the resulting shapers, it can be seen that the Two-Mode SI shaper, (40), is approximately 0.9 seconds longer in duration. This is because the SI has a higher robustness than the ZV shaper. The insensitivity of the SI shaper's two frequencies are $I = 0.55$ for the low mode and $I = 0.51$ for the high mode when the frequencies are normalized around the median value in each range. Designing for these frequency ranges resulted in a SI shaper that suppressed a continuous frequency range, while the ZV shaper allows the vibration of the system to increase to nearly 20% between the two design frequencies.

5.1.3 Experimental Results

5.1.3.1 Moving Around Obstacle

The hook response during a typical move to avoid the obstacle by moving around it is shown in Figure 39. The payload can be assumed, based on simulation data, to swing no more than 5 degrees, or 22 cm further than the hook. This justifies using the hook position data to give a reasonable estimate of payload response.

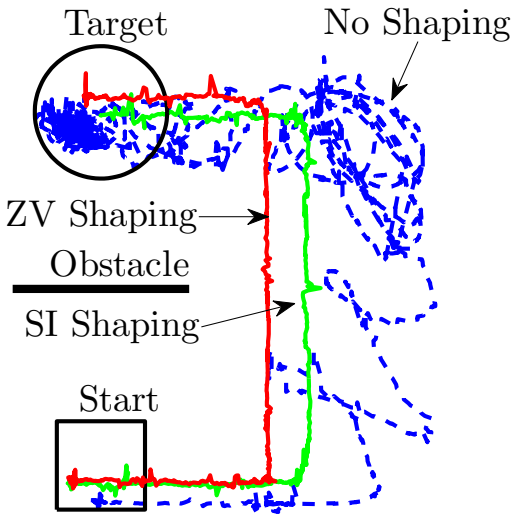

Figure 39: Typical Hook Response When Avoiding the Obstacle

It can be seen from the figure that without input shaping the system response oscillates a great deal, simultaneously increasing task completion time, operator effort, and decreasing safety. It also shows that the workspace the operator must utilize is larger than with input shaping enabled. Both input shapers do a good job of suppressing the vibration in the hook, allowing the operator to control the system more accurately. This allows the operator to move the system in a smaller workspace and exert less effort. The SI shaping path is wider than the ZV shaping path because the shaper duration of the SI shaper is longer than the ZV shaper.

The time to completion results are shown in Figure 40. When no input shaping was used, the completion times were much longer than with either type of input shaping. The average time to completion for the unshaped move was 149 seconds. When the task was completed with Two-Mode ZV shaping implemented on the controller, the average completion time was reduced to only 22.5 seconds. With ZV shaping, the operator was able to complete the task in 15.9% of the time required without the shaping. When the Two-Mode SI shaping was used to move the system, the

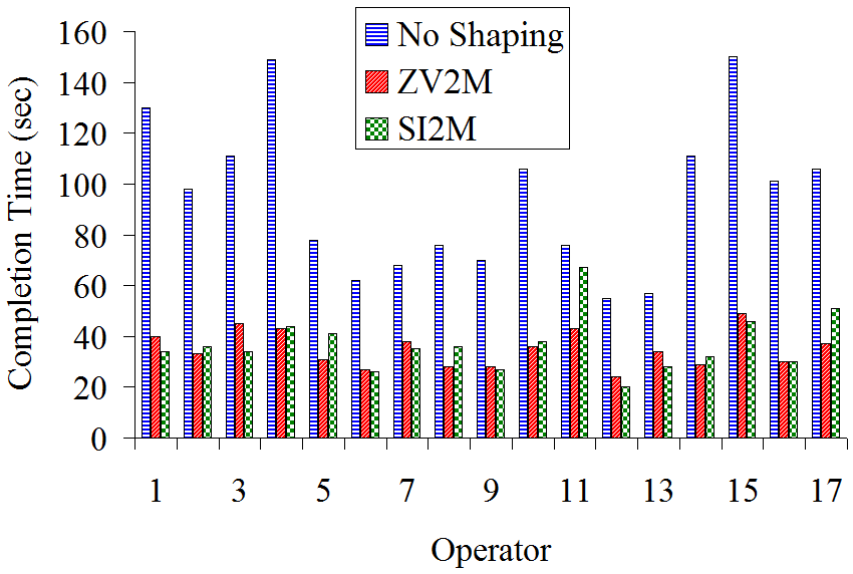

Figure 40: Time to Completion For Moving Around Obstacle

Table 5: Completion Times When Moving Around Obstacle

Shaper	Average Completion Time (sec)	Standard Deviation (sec)	Reduction
Unshaped	149	44	-
ZV 2 Mode	22.5	6.9	84%
SI 2 Mode	22.5	6.7	84%

average time to completion was also 22.5 seconds, again 15.9% of the time required to complete the move without the shaper. Table 5 summarizes these results. The standard deviation between the two shapers was very close, showing that the shaper results were almost identical. This shows that the more robust SI shaper can be used for this move with virtually no negative effect on completion time. However, the SI shaper offers more robust performance when the suspension length and payload characteristics change.

Figure 41 shows the operator effort, measured using the number of button pushes, required to move the payload around the obstacle. Without input shaping, the average number of button pushes needed to complete the task was 33. With Two-Mode ZV shaping turned on, the average number of times the operator need to push the buttons dropped to only 6. That is an 82% reduction in operator effort with the ZV shaper

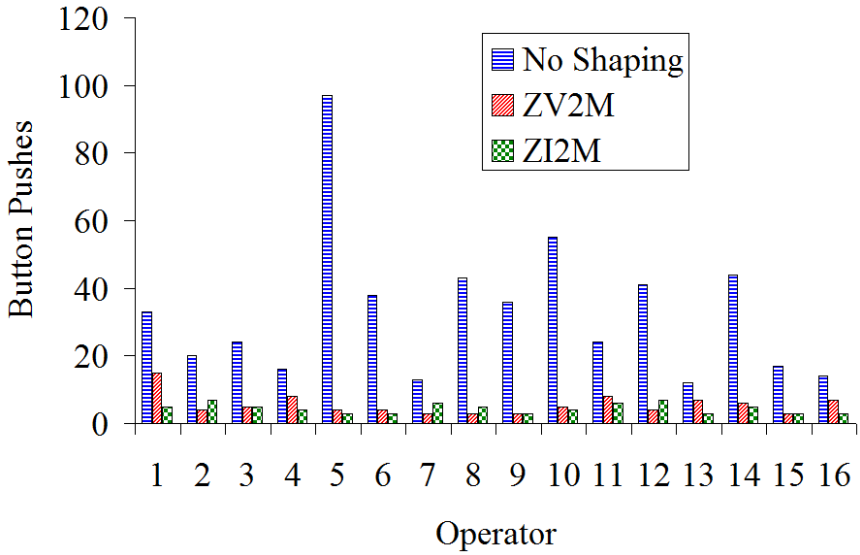

Figure 41: Operator Effort When Moving Around Obstacle

implemented. When Two-Mode SI shaping was used to move the system around the obstacle, the average number of button pushes was only 5. The operator effort with the use of the SI shaper was reduced by 85%. Therefore, both shapers greatly reduced the amount of operator effort to move the payload around the obstacle.

When an operator moves a crane in two-dimensions, they sometimes push two buttons on the pendent simultaneously, to move diagonally. Figure 42 shows the number of simultaneous button pushes. When no input shaping was used, only 25% of the operators felt comfortable moving the payload diagonally around the obstacle. For this group of operators, the average number of times they moved diagonally was 3, or 9% of the average total number of button pushes used to move the payload. When ZV shaping was used, the number of operators that moved diagonally around the obstacle increased to 50%, twice the number willing to move diagonally without input shaping. The average number of times these operators moved diagonally was 3. While the average number of times that this group of operators moved was the same, the percentage of simultaneous button pushes to the average total number of button pushes increased to 50%. When Two-Mode SI input shaping was used to move the

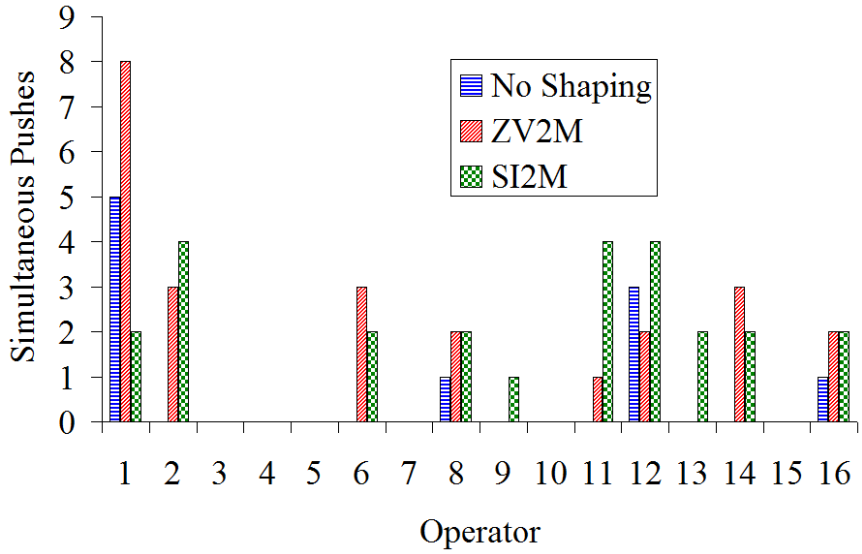

Figure 42: Simultaneous Button Pushes When Moving Around Obstacle

Table 6: Average Operator Effort When Moving Around an Obstacle

Shaper	Button Pushes	% Reduction	% Simultaneous Pushes
Unshaped	33	-	11%
ZV2M	6	82%	50%
SI2M	5	85%	60%

payload, the number of operators attempting to move diagonally around the obstacle increased to 62.5%. The average number of times the operators attempted to move diagonally was also 3. The percentage increase of overall operator effort used in diagonal moves increased to 60% of the average total effort exerted when using the SI shaper. These results are summarized in Table 6.

5.1.3.2 Hoisting Over Obstacle

Figure 43 shows typical hook responses when hoisting the payload over the obstacle. When there is no input shaping used to move the system, the hook and the payload oscillate a great deal. This makes it difficult for the operator to position the payload within the target zone and to determine how high off the ground the payload is. Hoisting the payload causes the frequencies of the system to change because the suspension length of the crane is decreasing when the payload is lifted over the obstacle

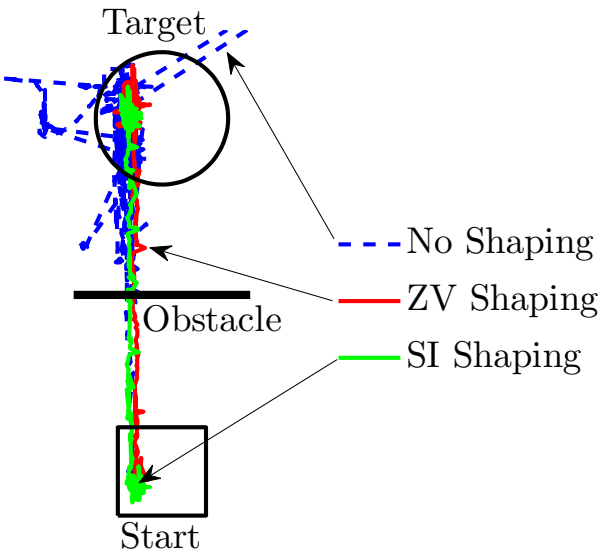

Figure 43: Typical Hook Response When Hoisting Over the Obstacle

and then increasing when lowering the payload into the target zone [56]. These changes result is a more dangerous work area because it is difficult for the operator to gage payload swing near the obstacle resulting in an increased possibility of collisions. The input shapers used for hoisting were the same ones used for moving around the obstacle. Both input shapers used on the system decreased the vibratory response of the system allowing for more accurate positioning of the payload and decreased the danger of collisions.

Figure 44 shows the amount of time each operator took to complete the task of hoisting the payload over the obstacle. The average time to completion without input shaping was 94 seconds. It took an average of only 35 seconds for the operators to move the payload to the target zone with the Two-Mode ZV shaper. The operators thus took 63% less time to complete the task with the ZV shaper suppressing the vibration in the system. Using the Two-Mode SI input shaper allowed the operator to complete the task in an average of only 37 seconds. Table 7 summarizes these results.

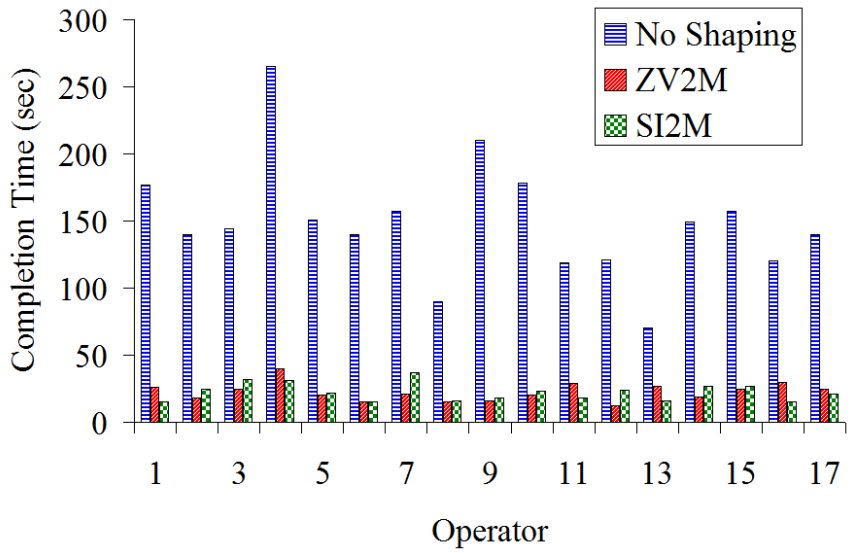

Figure 44: Time to Completion When Hoisting Over the Obstacle

Table 7: Average Completion Times When Hoisting Over the Obstacle

Shaper	Completion Time (sec)	Reduction
Unshaped	94	-
ZV 2 Mode	35	63%
SI 2 Mode	37	61%

The average completion time for the SI shaper was slightly larger than the ZV shaper completion time. The reason for the increased time when moving the payload with the SI shaper may be a result of the 1 second longer duration of the shaper.

Figure 45 shows that the average number of button pushes required to hoist the payload over the obstacle was 16 without shaping. Using either the Two-Mode ZV or Two-Mode SI shapers to suppress the vibration reduced the average number of button pushes to 4. This represents a 75% decrease compared to the unshaped case. Table 8 summarizes these results.

For 3 operators, the amount of effort required to move the payload without the input shaper was either equal to or lower than number of button pushes used when input shaping was enabled. For these cases in which the operators did not decrease their effort when input shaping was turned on, it can be seen in Figure 44 that the

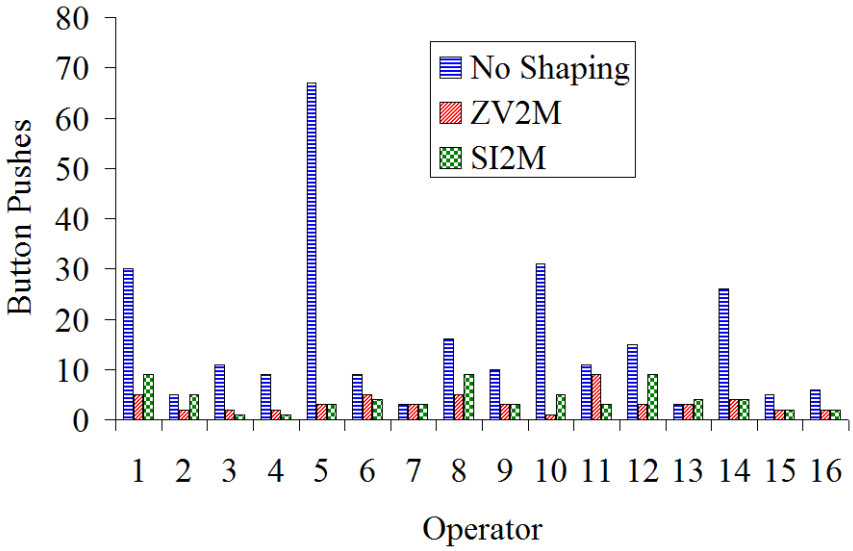

Figure 45: Operator Effort When Hoisting Over Obstacle

Table 8: Average Operator Effort When Hoisting Over an Obstacle

Shaper	Button Pushes	% Reduction
Unshaped	16	-
ZV2M	4	75%
SI2M	4	75%

operators still took a longer time to move the payload over the obstacle than when input shaping was used.

5.1.4 Discussion

Based on the results summarized in Tables 5 and 7 it can be seen that implementing either input shaper substantially reduces the task completion times. There was more than an 80% drop in completion time for moving around the obstacle and more than a 60% reduction in completion time for hoisting the payload over the obstacle. Part of the reason that the hoisting improvement was not as high as the obstacle avoidance task was that part of the move involved moving the payload vertically, which took equal time regardless of the control used. A crane operator with 30 years of experience also drove the crane through similar tasks. When not using input shaping, the operator took 33 seconds to move the payload around the obstacle. With

a two-mode SI shaper, the time to completion decreased to 27 seconds.

The operator effort reduction when using the input shapers was significant, 75% for the hoisting case and over 80% for the obstacle avoidance case, as summarized in Tables 6 and 8. It can be inferred from these reductions that the operators were more confident in their driving skills. This is also shown in the increased number of operators in the study that felt comfortable moving the payload diagonally around the obstacle. Because the hoisting task did not involve two-dimensional horizontal motion, there were no simultaneous button pushes. The reduction in operator effort indicates a saving in energy usage because the crane motors are not being actuated nearly as much for the same operation.

Figures 39 and 43 showed that a typical move for each task used a smaller workspace when utilizing input shaping. This allows for a more efficient use of floor space where the crane is being operated because the crane has a smaller danger zone.

Comparing the two input shapers, the ZV shaper had a shorter duration but did not significantly reduce the completion times compared to the SI shaper when comparing both to the unshaped case. The SI shaper was more robust that the ZV shaper, but because of the physical limits of the crane it was tested on, the robustness differences between the two shapers was not apparent.

5.1.5 Conclusions

Using either the Two-Mode ZV input shaper or the Two-Mode SI input shaper allowed operators to use a bridge crane to effectively avoid obstacles and accurately place distributed payloads in specified areas. The results found in this study compare very well to a similar study done by Kim and Singhose [28] on double pendulum point-mass payloads and with a study done on tower cranes [67]. The operating benefits of using a shaper included: decreased completion time, decreased operator effort, and a smaller danger of collisions.

5.2 Distributed Payload Crane Operator Learning Study

The last section showed that using input shaping to control an industrial bridge crane moving a distributed payload decreased the completion time of tasks, while also decreasing the operator effort and creating a safer work environment. This section investigates the long term effects of input shaping on an industrial bridge crane by studying operator learning. The purpose of this study was to determine how the operator's performance changed over time when operating the crane with a distributed payload.

Two tasks similar to the previous study were performed. In Task 1, the operator was required to pick up a payload, move around a corner, and set the payload down within a designated target zone. For Task 2, the operator hoisted a payload from the ground, over an obstacle, and set it down in a designated target zone. To study the effects of operator learning, the operators were required to conduct each task on eight different days during a two-week period.

5.2.1 Experimental Setup

Figures 46 and 47 show the courses for the two tasks performed by the operators. The goal of both tasks was to pick up an distributed payload form the start zone and set it down in a target zone, which was 20 cm longer and wider than the payload. Figure 48 shows a picture of the payload used in this study. The payload was designed to simulate large crates or cargo containers. The payload is 2.16 m long, by 1.5 m wide, and 0.31 m tall. Six mounting posts are positioned along the center cross-beams so that weights can easily be added and removed. The weights can be arranged in different configurations to simulate different payload weight distributions. The payload mass ranged from 53 kg, when only two weights were attached to the payload structure, to 75 kg, when four weights were attached. The different payloads were categorized by their radii of gyration. Because it is rectangular, the payload has two

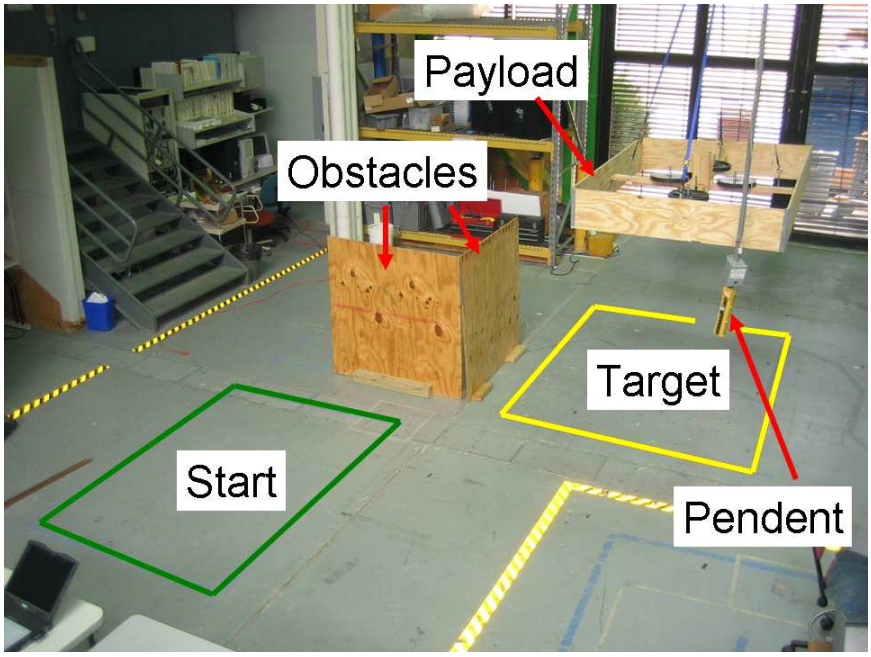

Figure 46: Picture of Corner Course

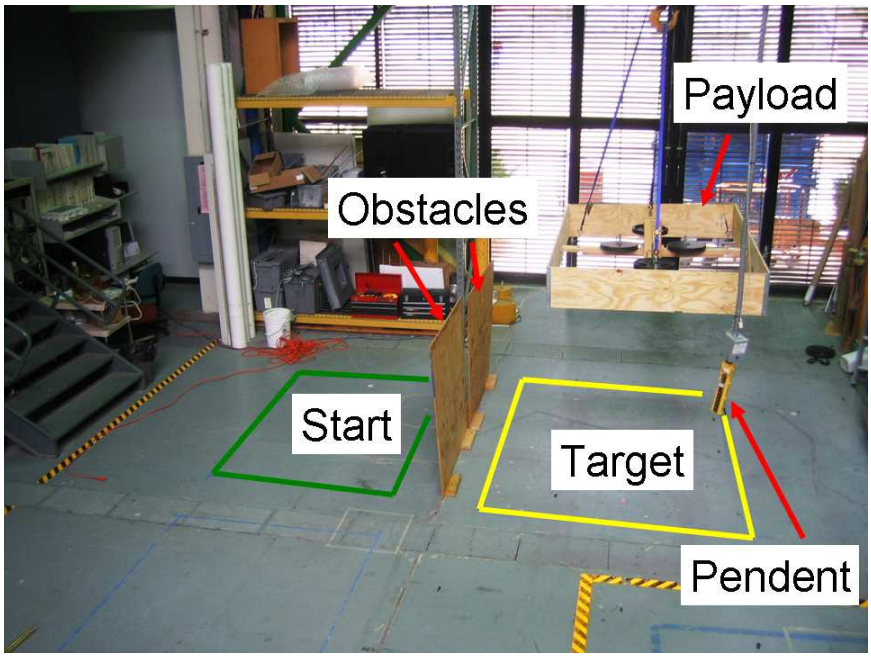

Figure 47: Picture of Hoisting Course

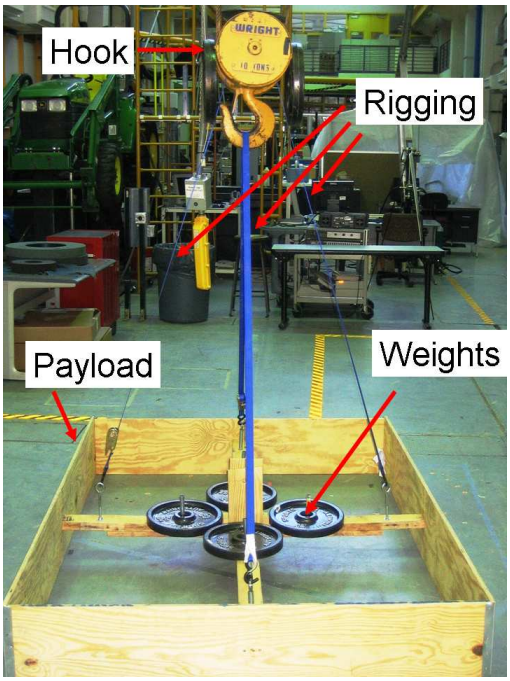

Figure 48: Payload Used in Operator Learning Study

radii of gyration. The radii of gyration ranged from 0.31 m to 0.73 m depending on the weight configurations. Four different payload distributions were used during the operator learning tests.

Figure 46 shows the avoidance course where the operator must move around the corner obstacle. The corner avoidance task was conducted to study the operator learning with two-dimensional swing. Task 2 is illustrated in Figure 47. The operator hoisted the payload over the obstacle and set it down in the target zone. This task was used to study the operator learning when the frequency of the payload swing changed.

The payload was suspended 1.8 m from the hook by four rigging cables attached to the ends of the payload cross-beams. The rigging cables were attached through the hook and over the hook to reduce twisting. The hook weighed 72 kg.

The operators used the pendent shown in Figure 37. They started each task with the payload resting on the floor. The operators picked up the payload, moved it to the target zone, and set it back down on the floor. The time to completion, from the

time the first button was pushed until the payload rested on the floor, was recorded. The number of times the operator hit the obstacles and the number of button pushes were recorded. After the payload was set on the ground, the positioning error was determined by measuring the maximum distance the payload was outside the target zone. The order of the tasks and the payload weight distributions were randomized.

Ten students at Georgia Tech volunteered to conduct the operator learning study. Each operator conducted the tasks with input shaping and without input shaping. Each trial took approximately a half-hour. Altogether, the operators conducted 40 hours of crane operations. This study was conducted with the help of Jeffrey Clement and Kelvin Chen Chih Peng.

5.2.2 Shaper Design

For this study, a ZV shaper and a Two-Mode SI shaper were designed for the manipulation tasks. The ZV shaper was designed to suppress the low mode in the system when the payload was 18 cm off the floor. The Two-Mode SI shaper was designed to suppress both modes exhibited by the system when the payload was suspended close to the floor, 18 cm, and when the payload was suspended above the obstacle, 1.2 m. The ZV shaper was designed using the constraint equations discussed in Chapter 1. The Two-Mode SI shaper was designed using the simple algorithm discussed in Chapter 3, using a vibration tolerance of 5%.

The frequencies used to design the two shapers were found using the frequency equations developed in Chapter 2. To verify these results, experiments on the crane were conducted for each payload used. The verification experiments were conducted in the same way as in the last section. The design frequencies are displayed in Table 9.

The ZV shaper used the median frequency of the low frequencies in the table. The

Table 9: Operator Learning Study Design Frequencies

Height off Floor	Low Frequency	High Frequency
18 cm	0.22 Hz	0.46 Hz
1.2 m	0.27 Hz	0.61 Hz

resulting shaper is:

$$\begin{bmatrix} A_i \\ t_i \end{bmatrix} = \begin{bmatrix} 0.5 & 0.5 \\ 0 & 2 \end{bmatrix} \quad \text{(ZV Shaper)} \tag{41}$$

The insensitivity of the ZV shaper at a $V_{tol} = 5\%$ is $I = 0.06$. This is a property of all ZV shapers regardless of design frequency.

The Two-Mode SI shaper was designed for the frequency ranges shown in Table 9. The resulting shaper is:

$$\begin{bmatrix} A_i \\ t_i \end{bmatrix} = \begin{bmatrix} 0.12 & 0.24 & 0.30 & 0.23 & 0.11 \\ 0 & 1.2 & 2.3 & 3.5 & 4.6 \end{bmatrix} \quad \text{(Two-Mode SI)} \tag{42}$$

The Two-Mode SI shaper is 2.6 seconds longer than the ZV shaper because it is suppressing two frequencies and has much better robustness. The insensitivities of the normalized modes for the Two-Mode SI shaper are $I = 0.2$ and $I = 0.28$.

5.2.3 Experimental Results

5.2.3.1 Corner Obstacle Avoidance

The average completion time results for the corner obstacle avoidance task are shown in Figure 49 as a function of trials completed by each operator. The figure also includes the standard deviation of each trial and the minimum time to completion. The minimum time to completion is the quickest possible completion time allowed by the actuators of the crane. These results incorporate the collisions and final position error in the form of time penalties added to the raw time completions. If the operator hit the obstacle, it resulted in a 5 second penalty. At the end of each task, the position

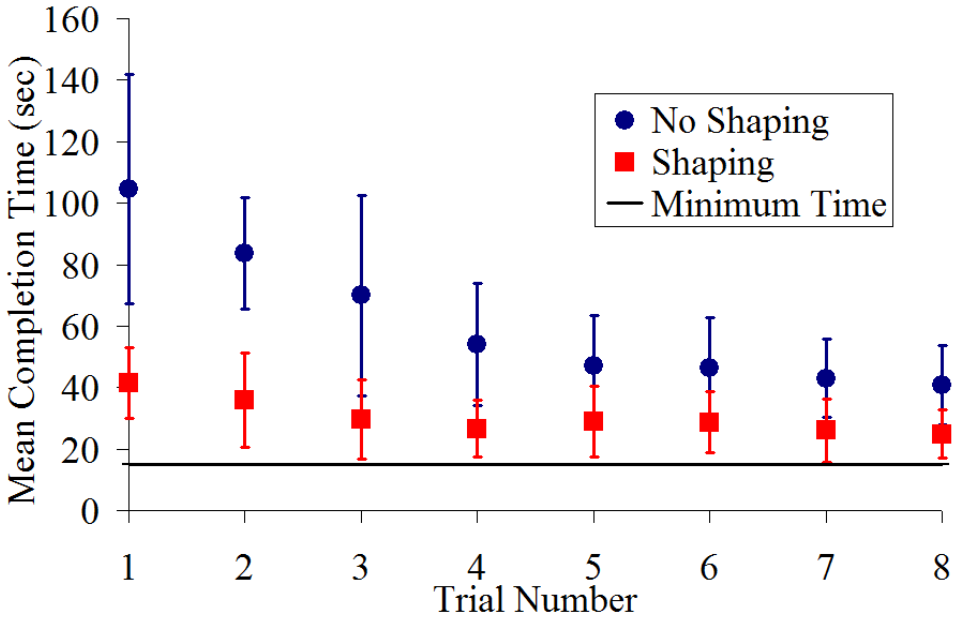

Figure 49: Corner Obstacle Avoidance Average Completion Times

error was measured and 2 seconds was added to the final time score for every 2.5 cm of position error. The penalties were developed through test runs of the study. It was found that it took about 2 seconds to adjust a payload 2.5 cm outside of the target zone. A 5 second penalty was assessed to discourage operators from using the obstacle to dampen the payload oscillations.

Without input shaping, the operators started with an average completion time over 100 seconds. As the operators conducted more trials during the two-week training period, they learned how to manage the payload, resulting in shorter completion times. Their improvement leveled off at around an average of 40 seconds. Using input shaping allowed the operator to start with a low completion time, 40 seconds, and keep it low with a final average time of 25 seconds. From Figure 49 it can be seen that without input shaping, the operators experienced a learning curve for operating the crane. With input shaping, there was a small learning curve, but overall the completion times did not decrease as drastically because, with input shaping enabled, all the operators were highly effective in their first trials. Without input shaping,

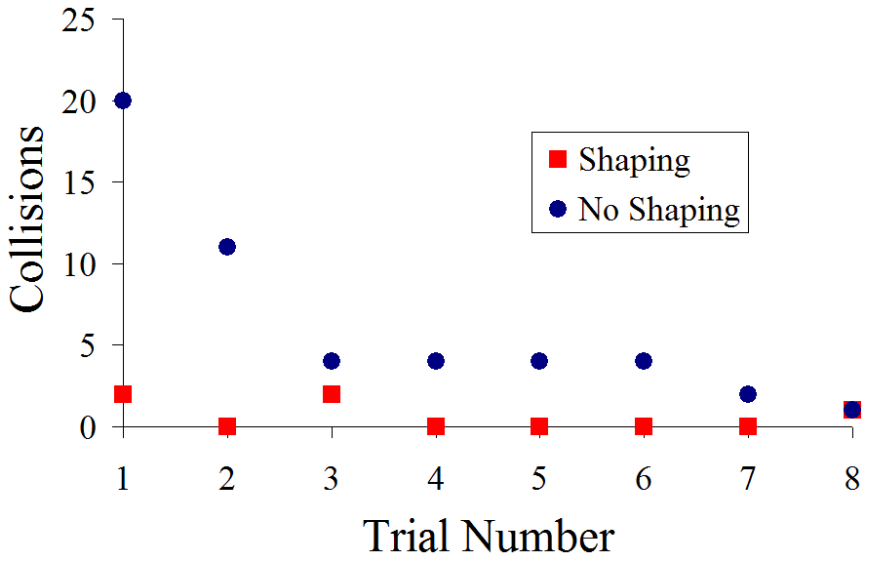

Figure 50: Corner Obstacle Avoidance Obstacle Collisions

the completion times vary significantly over all the trials, with standard deviations ranging from 13 seconds to 37 seconds. With input shaping, the completion times do not vary a great deal at the start of the trials and stay small throughout the trails, with standard deviations ranging from 8 to 15 seconds. Statistically, the P-value between the two average completion times is 0.005.

Figure 50 shows the total number of times all the operators collided with the obstacle during each trial. Without input shaping, the operators hit the obstacle ten times more than with input shaping when the trials started. As the operators conducted more trials, the operators improved in avoiding the obstacle, but continued to hit the obstacle more without input shaping. The obstacle was only hit a maximum of 2 times between the 10 operators when input shaping was used. By the end of the trails, the operators learned how to avoid the obstacle without input shaping but only improved to the level that the operators started at with input shaping enabled.

Figure 51 displays the average final positioning error when the operators placed the payload in the target zone. From this figure it can be seen that, initially, the operators had difficulty positioning the payload within the target zone without input

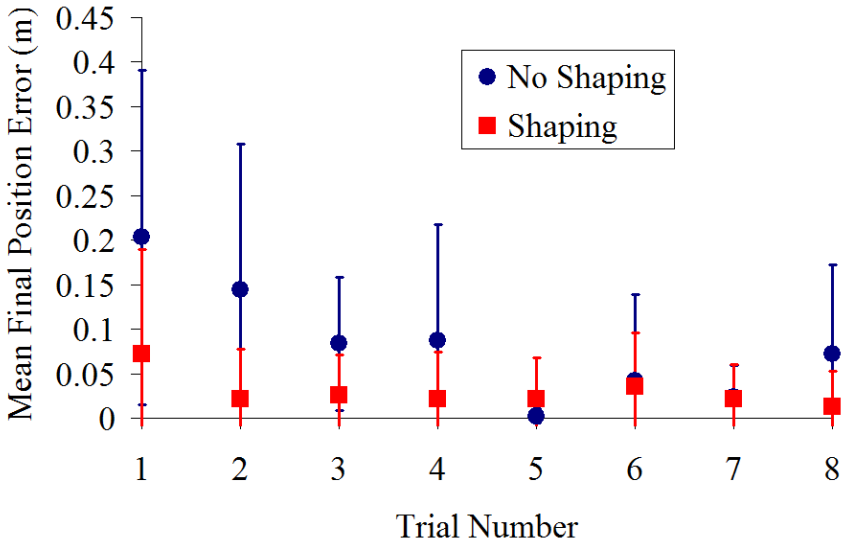

Figure 51: Corner Obstacle Avoidance Average Final Positioning Error

shaping, averaging 20 cm of error. As the operators conducted more tests, they were able to position the payload with more accuracy, but were unable to be consistently precise. With input shaping, the operators immediately had good positioning ability, averaging only 7 cm of error. Throughout the trails, the operators were able to keep a low final positioning error, with input shaping, ending with an average position error of only 1.3 cm during the eighth trial.

The hook move error is defined as the integral of the horizontal distance from the trolley center to the hook and is related to the size of the workspace required to safely move the payload. Figure 52 shows the average total hook position error accrued over the course of the move. This plot shows that when input shaping is not used, the hook moved an average of 9 m over the course of any given trial from its rest position directly under the trolley. As the operators conducted more trials, the hook error decreased, averaging 2 m of error, signifying that the operators were better able to keep the hook under the trolley and decrease the workspace that the operator needed to move the payload along with shorter completion times. With input shaping, the operator was better able to keep the hook under the payload under the trolley

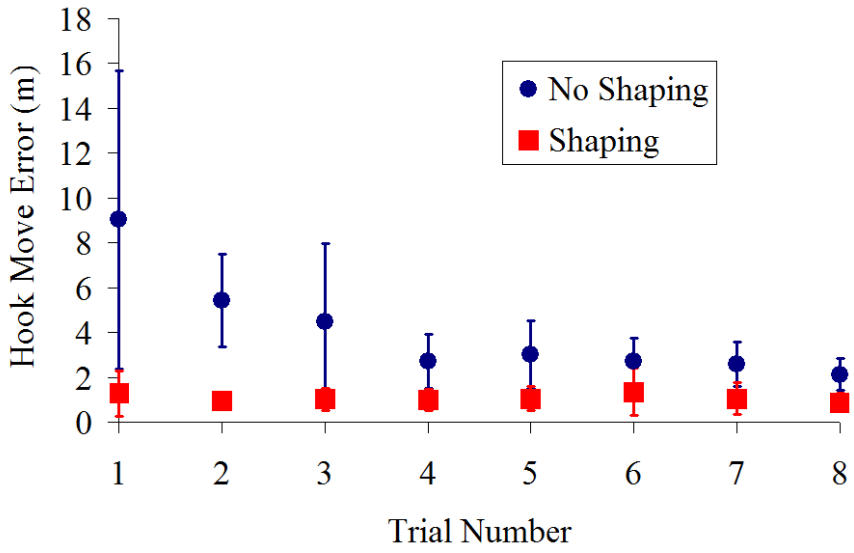

Figure 52: Corner Obstacle Avoidance Average Hook Move Error

throughout the trials than without shaping, with an average of only 1 m of hook error.

Figure 53 shows how the hook move error in the unshaped case was affected by the radius of gyration. Because the payload was rectangular, it had two different radii of gyration. When moving in the bridge direction the payload had a larger radius of gyration, and when moving in the trolley direction, a smaller one. When the operators first started the study (Trial 1), the hook move error was much larger for smaller radius of gyration, 5.5 m of hook error, than the large radius of gyration, 3.5 m of hook error. As the operators learned to control the payload the effects of the radius of gyration on the hook error decreased in both cases down to 1 m of hook error.

The average number of times that the operators pushed the pendent buttons is shown in Figure 54. With input shaping, the number of button pushes stayed low throughout the trials; staying below 12 button pushes. Without input shaping, the number of button pushes required by the operator to move the payload started out high, 36 pushes, and decreased as the operators conducted more trials, down to 10

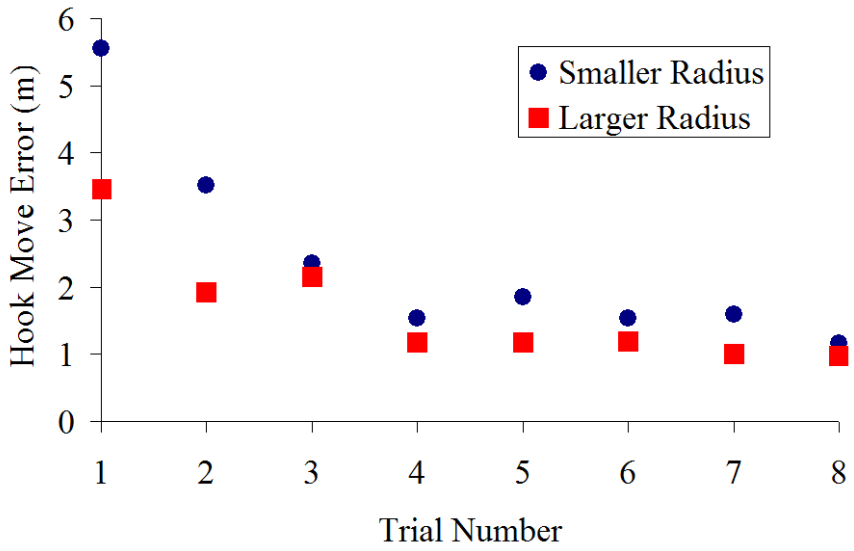

Figure 53: Corner Obstacle Avoidance Hook Move Error by Radius of Gyration

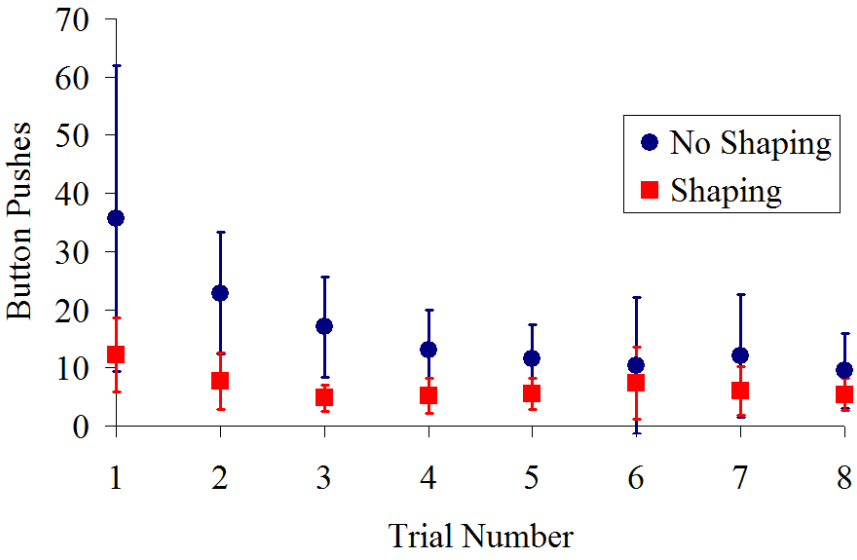

Figure 54: Corner Obstacle Avoidance Average Button Pushes

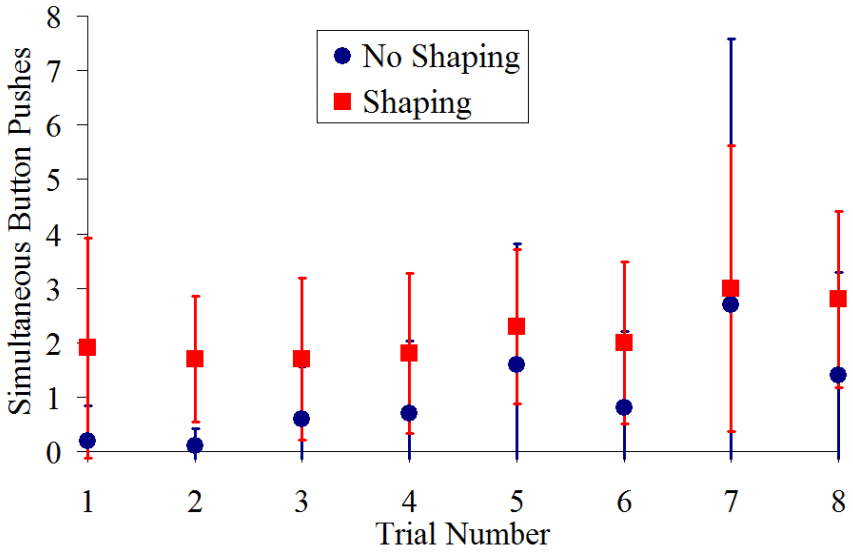

Figure 55: Corner Obstacle Avoidance Average Simultaneous Button Pushes

pushes. This figure shows that with input shaping, the operators were more efficient than without input shaping.

Figure 55 shows the average number of times the operator pushed two buttons simultaneously. This action results in a diagonal move that can decrease the transport path and shorten task completion time. At the start of the trials, most operators did not push buttons simultaneously when input shaping was disabled. As the trials continued, the operators started moving diagonally more often, up to about 15 simultaneous button pushes between the 10 operators. The spike in simultaneous button pushes in trial 7 for the unshaped case can be attributed to one operator who held down one button and tapped another button many times. With input shaping, the operator started out moving diagonally more often, and as the trials continued, increased the number of times that they moved diagonally.

5.2.3.2 Hoisting

Figure 56 displays the average completion times for the hoisting task. The data again incorporates the collision penalty and final position penalty in the final completion times. When input shaping was not used, the operators started off with a slow

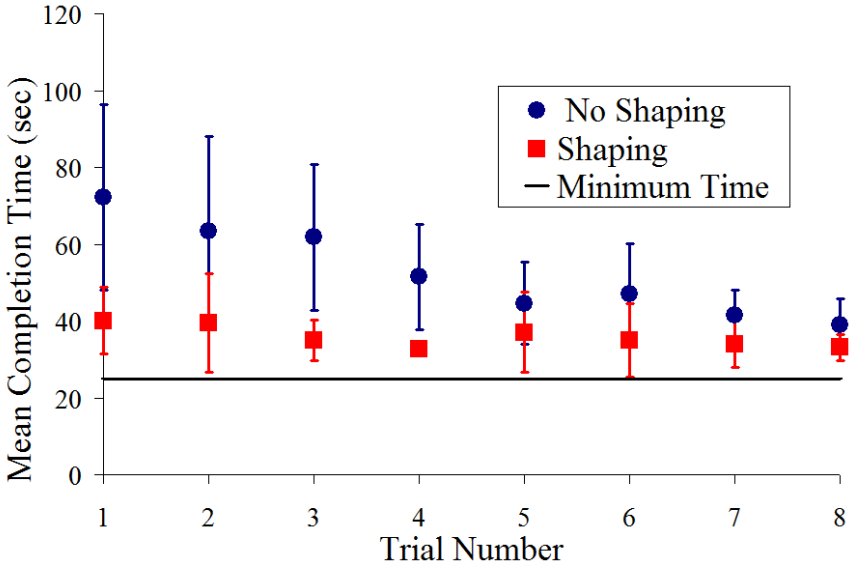

Figure 56: Hoisting Average Completion Times

completion time and improved by 46% by the end of the trials. With input shaping, the operators started out with fast completion times and kept the completion time curve relatively flat throughout the study with only a 17% decrease in completion time by the eighth trail. The P-value for the average hoisting completion times is 0.043.

The total number of times that the operators hit the obstacle during the hoisting task is shown in Figure 57. When using input shaping, the number of times the operators hit the obstacle stayed at or below 1. That is for any given trial, the obstacle was only hit once during all the 10 operator tests. Conversely, without input shaping, the operators hit the obstacle 7 times at the start of the study and continued to have multiple collisions until the very end of the training period.

Figure 58 shows the average final positioning error of the payload. During the first trial, the operators had average positioning errors of approximately 1 cm both with and without input shaping. Throughout the rest of the study, the positioning error for the operators without input shaping fluctuated by 700%. When input shaping was used, the operators started off with the low positioning error and kept it low,

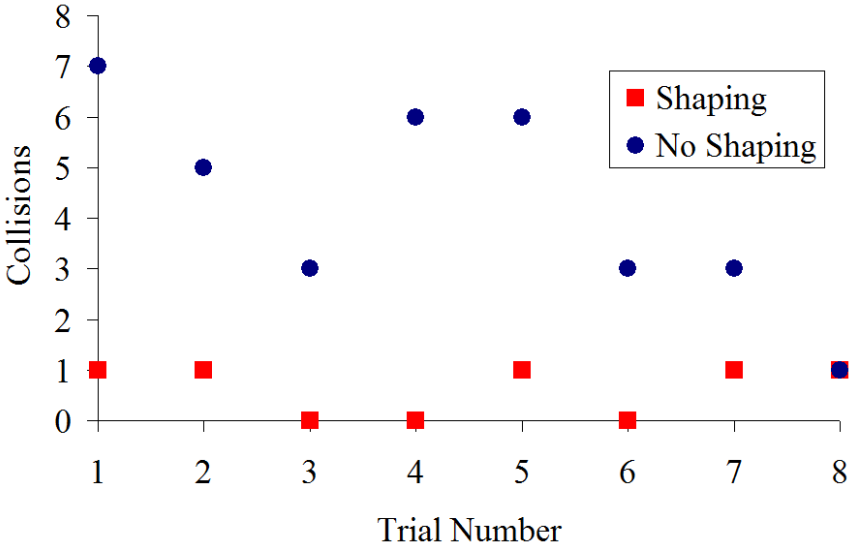

Figure 57: Hoisting Obstacle Collisions

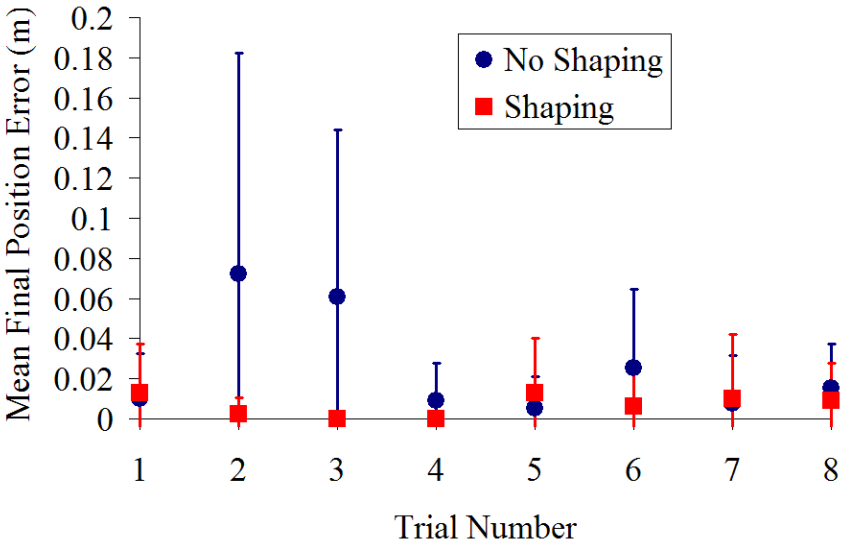

Figure 58: Hoisting Average Final Position Error

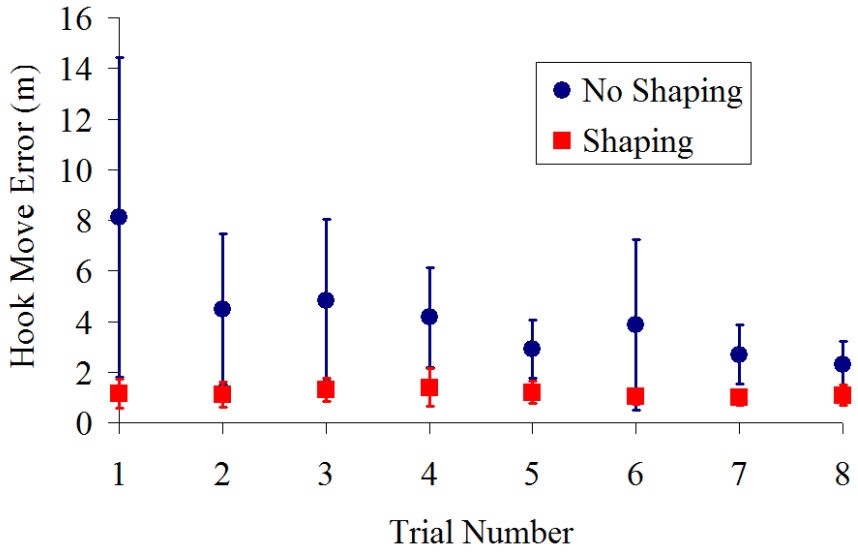

Figure 59: Hoisting Average Hook Move Error

only averaging a 2 cm error in the worst case. This result shows that, with input shaping, the operators were able to consistently and accurately position the payload in the target zone.

Figure 59 displays the average error in hook position over the whole hoisting manoeuver. When input shaping was used, the hook stayed closer to the trolley position resulting in a 1 m hook position error. When input shaping was not used, the average error started out at more than 8 m, but as the operators learned to control the payload while hoisting, the error decreased to 2 m. With input shaping, the operator started out being better able to control the payload and had better control of the payload over the entire study.

The average number of times the operators pushed the pendent buttons while moving the payload is displayed in Figure 60. When the operators started the study, the operators without input shaping exerted a large amount of effort to move the payload over the obstacle, averaging 22 button pushes. As the operators conducted more trials, the operator effort decreased to 7 pushes. With input shaping, the operators exerted less operator effort during the entire study. The average number of

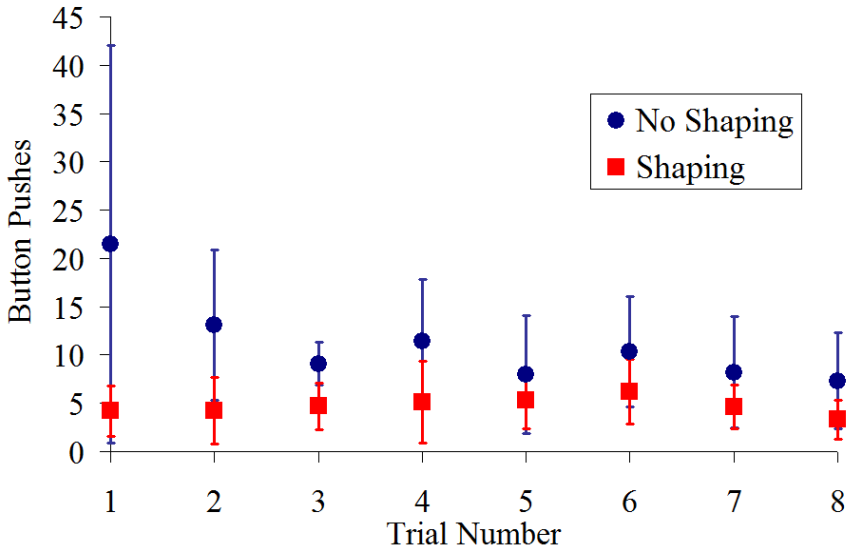

Figure 60: Hoisting Average Button Pushes

button pushes stayed relatively constant at approximately 5 throughout the study.

5.2.4 Discussion

The average task completion time results shown in Figures 49 and 56 show that operators exhibit a significant learning curve when driving an industrial bridge crane with a distributed payload without input shaping. As the operator conducts more trials the improvement between trials decreases, represented by the curves flattening out and approaching a lower bound. When input shaping is used, the operators were immediately able to rapidly complete both tasks. Therefore, there was a small amount of learning at the beginning of the study, but the curves flattened out quickly near the theoretical lower bound governed by the acceleration and velocity limits of the crane. While a few of the operators were able to occasionally complete the tasks almost as quickly without the input shaper as with the shaper, on average, the operators without input shaping were never able to approach the performance achieved with input shaping.

The collision data for both tasks, seen in Figures 50 and 57, shows a similar trend to the completion times. When the trials began, the operators frequently hit the

obstacles when not using the input shaper. As the operators continued the trials, they learned how to avoid the obstacles. It was observed that, when hoisting, the operators had a tougher time gauging the position of the payload relative to the top of the obstacle. This resulted in more hits as the operator attempted to move over the obstacle into the target zone. To avoid hitting the obstacle, the operators started to make wider moves around and over the obstacle, or slowed down the payload when approaching the obstacle. By the end of the study, the operators learned to avoid the obstacles without input shaping, as well as with input shaping.

Given the inherent difficulty of the tasks, there was positioning error in many cases, as shown in Figures 51 and 58. Without input shaping, the final position of the payload out of the target zone was higher when the study started and decreased to the level possible with input shaping. It was observed that as the operators progressed through their training, they would start to set part of the payload down in the target zone and allow the payload to rotate back and forth over the target zone. When the payload was completely within the target zone, the operator would then quickly drop the payload to the floor. If the operator timed the drop correctly, then the payload would be wholly within the target zone. When input shaping was used, some operators would start to set the payload down too early, trying to decrease the completion time of the task, and leave part of the payload outside the target zone. However, overall the positioning errors were very small when input shaping was utilized.

The average number of times the operator pushed the buttons on the pendent to complete each task is related to the amount of mental and physical effort the operator exerted to complete each task. It can be inferred from the data that the more the operator had to push the buttons to control the payload, the more the operator had to concentrate on the payload motion. Figures 54 and 60 show that as the operator conducted more trials, the operator effort for the unshaped tasks decreased. However,

input shaping allowed the operators to exert much less effort to move the payload to the target zone throughout the training. For the corner obstacle avoidance task, the operator was able to conduct simultaneous button pushes to create diagonal moves, as seen in Figure 55. As the operators conducted more trials, the number of time-saving diagonal moves increased. The operators moved the payload diagonally more with input shaping than without. When asked about this, many of the operators said that they felt more comfortable moving diagonally with the input shaper than without it. This seems to indicate that with input shaping enabled, operators are more comfortable making complicated moves.

The average error in hook positioning over the course of each move was plotted in Figures 52 and 59. This tracking error can be related to the size of the manoeuver zone required to move the payload safely. When input shaping was used, the average hook positioning error stayed under 2 m for the entire study for both tasks. When the operators moved the payload without input shaping, the operators started out with more than 8 m of hook error. As the operators completed more trials, the error decreased and flatted out at 2 m, which is where the shaped tasks started out. This suggests that the manoeuvering zone required for the average operator is much smaller with input shaping than without input shaping.

The effects of different radius of gyrations on the tasks was seen in Figure 53. When the operators started the study, the differing frequencies and amplitudes introduced by the different radii of gyration affected the hook position the most. As the operator learned how to control the payload, the effect of the payload radii on the control of the payload decreased. The small radius of gyration caused more error than the large radius of gyration. These results agree with the dynamic analysis conducted in Chapter 2. In that chapter, it was found that when the radius of gyration gets larger, the payload is more resistant to large payload oscillations, resulting in smaller payload swing amplitudes. As the radius of gyration gets smaller, the payload and

hook act more like a point-mass double pendulum, and since the mass ratio for this study ranged from 0.74 and 1.04, the oscillation amplitude contributions from the non-dominant mode when the radius of gyration was small increased.

5.2.5 Conclusions

From this study it can be concluded that using an input shaper results in faster completion times, more accurate positioning, less obstacle-payload collisions, smaller manoeuver zones, and less operator effort. When operators do not use input shaping, they learn how to increase their efficiency over time. With input shaping, the novice operator is already as proficient as an experienced operator. The payload radius of gyration affects the move error for new operators without input shaping, but as the operator learns, the effects of the radius of gyration decreases. Even with substantial training, crane operators driving an unshaped crane cannot approach the overall performance of completely novice operators driving a crane equipped with input shaping.

CHAPTER VI

CONCLUSIONS AND FUTURE WORK

Every machine vibrates and an important subclass of machinery are two-mode flexible systems. This thesis presented ways of improving the control of two-mode flexible systems using input shaping. These machines are used in many facets of industry, ranging from massive cranes used in shipyards to pick-and-place flexible robotic arms used in assembly plants.

Chapter 1 of this thesis explained the input shaping method and reviewed two simple shapers, Zero Vibration (ZV) and Zero Vibration and Derivative (ZVD) shapers. ZV shapers are not robust and ZVD shapers do not allow the designer to select the insensitivity ranges to create an optimal shaper.

An in-depth dynamic analysis of cranes moving distributed payloads was presented in Chapter 2. Equations for determining the frequencies and amplitude contributions of each mode were developed for generalized payloads, enabling any payload/crane system to be analyzed. It was shown that the frequencies of a distributed payload crane decrease as the radius of gyration increases or the rigging length increases in proportion to the total length of the system. The amplitude contributions of each frequency to the impulse response of the system vary with rigging length and the radius of gyration of the payload. As the radius of gyration increases, the dominant mode changes from the low mode of the system to the high mode of the system. This is because as the radius of gyration increases, so does the inertia, while the moment being applied to the payload remains unchanged. It was found that the mass of the payload only affects the system when the radius of gyration is small.

Chapter 3 reviewed Specified Insensitivity (SI) shapers and introduced a new parameter optimization technique, Varying Amplitude Contribution Specified Intensity (VACSI) shapers. The insensitivity of SI shapers are chosen by the designer, allowing for a specific range of frequencies to be suppressed. SI shapers also relax the vibration constraint by allowing a small tolerable amount of residual vibration. VACSI shapers take advantage of the amplitude contribution of each mode to optimize the vibration tolerances for each frequency. VACSI shapers were shown to have lower shaper durations than two-mode SI shapers when the insensitivity of the dominant mode was smaller than the insensitivity of the non-dominant mode.

Chapter 4 presented experimental results from two different types of industrial machinery, a two-link flexible robotic arm and a 10-ton industrial bridge crane. The experimental results agreed with the analysis presented Chapter 3. Chapter 5 presented two operator studies which explored two aspects of operator interaction with input shaping. The first study investigated differences between ZV shaping and SI shaping along with operator improvements when using input shaping. The second study examined the effects of operator learning with and without input shaping. Both studies examined the affects of distributed payloads on the operator's efficiency.

This research has exposed numerous important question that could be the subject of future work. A modal analysis of distributed payload cranes and two-link robot arms can be conducted to study the specific mode shapes and study the scaling of the inputs. The VACSI shaper algorithm can be extended to negative input shapers to investigate the effects of these more aggressive input shapers. Operator studies can be conducted on larger cranes in order to use payloads with larger radii of gyration and larger hoist distances and more complicated tasks. This would also allow for more distinction to be made between ZV shapers and SI shapers. The effects of changing velocity limiting on operators with distributed payloads can be investigated. Test could be run combining hoisting and 2 dimensional motion to further investigate the

effects of hoisting on more complicated motion.

Although significant future work is possible, A deeper understanding of distributed payload crane dynamics has been presented in this thesis. SI input shaping has been improved by intelligently designing the shaper through VACSI input shaping, and this thesis has firmly established that two-mode SI input shaping can substantially improve the performance of machines with two flexible modes.

REFERENCES

[1] Auernig, J. and Troger, H., "Time optimal control of overhead cranes with hoisitng of the load," *Automatica*, vol. 23, no. July, pp. 437–466, 1987.

[2] Banerjee, A., Pedreiro, N., and Singhose, W., "Vibration reduction for flexible spacecraft following momentum dumping with/without slewing," *Jornal of Guidance, Control, and Dynamics*, 2001.

[3] Bascetta, L. and Rocco, P., "End-point vibration sensing of planar exible manipulators through visual servoing," *Mechatronics*, vol. 16, pp. 221–232, 2006.

[4] Benosman, M. and Le Vey, G., "Control of flexible manipulators: A survey," *Robotica*, vol. 22, pp. 533–545, 2004.

[5] Bhat, S. and D.K., M., "Precise point-to-point positioning control of flexible structures," *ASME Journal of Dynamic Systems, Measurement, and Control*, vol. 112, no. 4, pp. 667–674, 1990.

[6] Bolz, R. E. and Tuve, G. L., *CRC Handbook of Tables for Applied Engineering Science*. Boca Raton, FL: CRC Press, Inc., 1973.

[7] Book, W. J. and Obergfell, K., "Practical models for practical flexible arms," in *IEEE International Conference on Robotics and Automation*, (San Francisco, CA), IEEE, 2000.

[8] Book, W. J. and Rhim, S., "Adaptive time-delay command shaping filter for flexible manipulator control," *IEEE/ASME TRANSACTIONS ON MECHATRONICS,*, vol. 9, no. 4, pp. 619–627, 2004.

[9] Butler, H., Honderd, G., and Amerongen, J., "Model reference adaptive control of a gantry crane scale model," *IEEE Control Systems*, vol. 11, no. January, pp. 57–62, 1991.

[10] Christian, A. and Seering, W., "Initial experiments with a flexible robot," in *IEEE Int. Conf. on Robotics and Automation*, (Cincinnati, OH), 1990.

[11] Craig, J. J., *Introduction to Robotics Mechanics and Control*. Reading, MA: Addison-Wesley Publishing Co., 2nd ed., 1986.

[12] Crain, E., Singhose, W., and Seering, W., "Evaluation of input shaping on configuration dependent systems," in *Japan-USA Symposium on Flexible Automation*, (Boston, MA.), 1996.

[13] Drapeau, V. and Wang, D., "Verification of a closed-loop shaped-input controller for a five-bar-linkage manipulator," in *IEEE Int. Conf. on Robotics and Automation*, (Atlanta), 1993.

[14] Economou, D., Mavroidis, C., Antoniadis, I., and Lee, C., "Maximally robust input preconditioning for residual vibration suppression using low-pass fir digital filters," *ASME Journal of Dynamic Systems, Measurement and Control*, vol. 124, pp. 85–97, 2002.

[15] Forest, C., Frakes, D., and Singhose, W., "Input-shaped control of gantry cranes: Simulation and curriculum development," in *ASME DETC 18th Biennial Conf. on Mechanical Vibration and Noise*, (Pittsburgh, PA), DETC2001/VIB-21522, 2001.

[16] Grosser, K. and Singhose, W., "Command generation for reducing perceived lag in flexible telerobotic arms," *JSME International Journal*, vol. 43, no. 3, pp. 755–761, 2000. journal.

[17] Grosser, K. E., *Input Shaping for Telerobotic Manipulators*. Masters, Georgia Institute of Technology, 2000.

[18] Hillsley, K. and Yurkovich, S., "Vibration control of a two-link flexible robot arm," in *IEEE International Conference on Robotics and Automation*, pp. 2121–26, 1991.

[19] Hong, K.-T. and Hong, K.-S., "Input shaping and vsc of container cranes," in *IEEE International Conference on Control Applications*, (Taipei, Taiwan), pp. 1570–1575, 2004.

[20] Huey, J. R. and Singhose, W., "Concurrent design of outside-the-loop input shaping and pid feedback control," 2006.

[21] Hyde, J. and Seering, W., "Using input command pre-shaping to suppress multiple mode vibration," in *IEEE International Conference on Robotics and Automation*, (Sacramento, CA), pp. 2604–2609, 1991.

[22] Kane, T. R. and Levinson, D. A., *AUTOLEV User's Manual, Online*. 1999.

[23] Kenison, M. and Singhose, W., "Input shaper design for double-pendulum planar gantry cranes," in *IEEE Conference on Control Applications*, (Kona, Hawaii), pp. 539–44, 1999.

[24] Khalid, A., Huey, J., Singhose, W., Lawrence, J., and Frakes, D., "Human operator performance testing using an input-shaped bridge crane," *ASME J. of Dynamic Systems, Measurement, and Control*, vol. 128, no. 4, pp. 835–841, 2006.

[25] Khalid, A., Singhose, W., Huey, J., Lawrence, J., and Frakes, D., "Study of operator behavior and performance using an input-shaped bridge

crane," in *IEEE Conference on Control Applications*, vol. 1, (Taipei, Taiwan), pp. 759–64, IEEE, 2004.

[26] Khorrami, F., Jain, S., and Tzes, A., "Experiments on rigid body-based controllers with input preshaping for a two-link flexible manipulator," in *IEEE Transactions on Robotics and Automation*, 1994.

[27] Kim, D. and Singhose, W., "Reduction of double pendulum crane oscillations," in *Eigth International Conference on Motion and Vibration Control*, (Daejeon, Korea), 2006.

[28] Kim, D. and Singhose, W., "Human operator learning on double-pendulum bridge cranes," in *ASME International Mechanical Engineering Congress and Exsposition*, (Seattle, WA), 2007.

[29] Lee, J., *Dynamic Analysis and Control of Lightweight Manipulators with Flexible Parallel Link Mechanisms.* PhD thesis, Georgia Institute of Technology, 1990.

[30] Liu, K.-P. and Li, Y.-C., "Vibration suppression for a class of flexible manipulator control with input shaping technique," in *Proceedings of the Fifth International Conference on Machine Learning and Cybernetics*, vol. 2006, (Dalian), pp. 835–839, 2006.

[31] Love, L., Magee, D. P., and Book, W. J., "A comparison of joint control algoritms for teleoperated pick and place tasks using a flexible manipulator," in *IEEE International Conference on Systems, Man, and Cybernetics*, (San Antonio, TX, USA), 1994.

[32] Magee, D. P. and Book, W. J., "Eliminating multiple modes of vibration in a flexible manipulator," in *IEEE International Conference on Robotics and Automation*, vol. 2, (Atlanta, GA), pp. 474–479, IEEE, 1993.

[33] Magee, D. P. and Book, W. J., "Filtering micro-manipulator wrist commands to prevent flexible base motion," in *American Control Conf.*, (Seattle, WA), pp. 924–928, 1995.

[34] Magee, D. P. and Book, W. J., "Optimal filtering to minimize the elastic behavior in serial link manipulators," in *American Control Conference*, (Philadelphia, PA), 1998.

[35] Mills, B., *Input Commands for Moving Flexible Systems without Residual Vibration*. Bacheolors, MIT, 1999.

[36] Murphy, B. and Watanabe, I., "Digital shaping filters for reducing machine vibration," *IEEE Transactions on Robotics and Automation*, vol. 8, no. April, pp. 285–289, 1992.

[37] Nho, H. C. and Meckl, P., "Intelligent feedforward control and payload estimation for a two-link robotic manipulator," *IEEE/ASME TRANSACTIONS ON MECHATRONICS,*, vol. 8, no. 2, pp. 277–283, 2003.

[38] Obergfell, K., *End-Point Position Sensing and Control of Flexible Multi-Link Manipulators*. PhD thesis, Georgia Institute of Technology, 1998.

[39] Oke, G. and Istefanopulos, Y., "Tip position control of a two-link exible robot manipulator based on nonlinear deection feedback," *Chaos, Solitons and Fractals*, vol. 17, pp. 499–504, 2003.

[40] Park, B. J., Hong, K.-S., and Huh, C., "Time-efficient input shaping control of container cranes," in *International Conference on Control Applications*, (Anchorage, AK), pp. 80–85, 2000.

[41] Park, K.-J., "Flexible robot manipulator path design to reduce the endpoint residual vibration under torque constraints," *Journal of Sound and Vibration*, vol. 275, p. 10511068, 2004.

[42] Rattan, K. and Feliu, V., "Feedforward control of flexible manipulators," in *Aerospace and Electronics Conference, 1991. NAECON 1991*, (Dayton, OH), 1991.

[43] Rhim, S. and Book, W. J., "Adaptive command shaping using adaptive filter approach in time domain," in *American Control Conference*, (San Diego, California), pp. 81–85, 1999.

[44] Romano, M., Agrawal, B. N., and Bernelli-Zazzera, F., "Experiments on command shaping control of a manipulator with flexible links," *Journal of Guidance, Control, and Dynamics*, vol. 25, no. 2, pp. 232–239, 2002.

[45] Sanz, A. and Etxebarria, V., "Experimental control of a two-dof flexible robot manipulator by optimal and sliding methods," *Intelligent Robot Systems*, vol. 46, pp. 95–110, 2006.

[46] Sato, K. and Sakawa, Y., "Modeling and control of flexible rotary crane," *International Jornal of Control*, vol. 48, no. 5, pp. 2085–2105, 1988.

[47] Siciliano, B., "Closed-loop inverse kinematics algorithm for constrained flexible manipulators under gravity," *Journal of Robotic Systems*, vol. 16, no. 6, pp. 353–362, 1999.

[48] Siciliano, B., "Pd control with on-line gravity compensation for robots with elastic joints: Theory and experiments," *Automatica*, vol. 41, p. 1809 1819, 2005.

[49] Singer, N. and Seering, W., "Preshaping command inputs to reduce system vibration," *ASME Journal of Dynamic Systems, Measurement, and Control*, vol. 112, pp. 76–82, 1990.

[50] Singer, N. and Seering, W., "An extension of command shaping methods for controlling residual vibration using frequency sampling," in *IEEE International Conference on Robotics and Automation*, (Nice, France), 1992.

[51] Singer, N., Singhose, W., and Kriikku, E., "An input shaping controller enabling cranes to move without sway," in *ANS 7th Topical Meeting on Robotics and Remote Systems*, (Augusta, GA), pp. 225–31, 1997.

[52] Singer, N., Singhose, W., and Seering, W., "Comparison of filtering methods for reducing residual vibration," *European Journal of Control*, vol. 112, pp. 76–82, 1999.

[53] Singhose, W., *Command Generation for Flexible Systems*. Phd, Massachusetts Institute of Technology, 1997.

[54] Singhose, W., "Trajectory planning for flexible robots," in *CRC Robotics and Automation Handbook* (Kurfess, T. R., ed.), pp. 9–1 – 9–24, CRC Press, 1st ed., 2004.

[55] Singhose, W., Kim, D., and Kenison, M., "Input shaping control of double-pendulum bridge crane oscillations," *ASME Journal of Dynamic Systems, Measurement, and Control*, vol. In Press, 2008.

[56] Singhose, W., Porter, L., Kenison, M., and Kriikku, E., "Effects of hoisting on the input shaping control of gantry cranes," *Control Engineering Practice*, vol. 8, no. 10, pp. 1159–1165, 2000.

[57] Singhose, W., Seering, W., and Singer, N., "Residual vibration reduction using vector diagrams to generate shaped inputs," *ASME Journal of Mechanical Design*, vol. 116, no. June, pp. 654–659, 1994.

[58] Singhose, W., Singer, N., and Seering, W., "Time-optimal negative input shapers," *ASME Journal of Dynamic Systems, Measurement, and Control*, vol. 119, no. June, pp. 198–205, 1997.

[59] Singhose, W. and Towell, S., "Input shaper design for double-pendulum planar gantry cranes," in *Double-Pendelum Gantry Crane Dynamics and Control*, 1998.

[60] Singhose, W., Vaughan, J., Danielson, J., and Lawrence, J., "Using tele-operated cranes for advanced controls education," in *ASME International Mechanical Engineering Congress and Exposition*, (Seattle, Washington), 2007.

[61] Smith, O., *Feedback Control Systems*. New York: McGraw-Hill Book Co., Inc., 1958.

[62] Sorensen, K., Singhose, W., and Dickerson, S., "A controller enabling precise positioning and sway reduction in bridge and gantry cranes," *Control Engineering Practice*, 2006.

[63] Sorensen, W., *A Combined Feekback and command Shaping Controller for Improving Positioning and Reducing Cable Sway in Cranes*. Masters, Georgia Institute of Technology, 2005.

[64] Tallman, G. H. and Smith, O. J. M., "Analog study of dead-beat posicast control," *IRE Transactions on Automatic Control*, no. March, pp. 14–21, 1958.

[65] Tuttle, T. and Seering, W., "Experimental verification of vibration reduction in flexible spacecraft using input shaping," *J. of Guidance, Control, and Dynamics*, vol. 20, no. 4, pp. 658–664, 1997. Command Shaping.

[66] Tzes, A. and Yurkovich, S., "Adaptive precomepsators for flexible-link manipulator control," in *28th Conference on Decision and Control*, (Tampa, FL), 1989.

[67] Vaughan, J., Kim, D., and Singhose, W., "Control of tower cranes with double-pendulum payload dynamics," *IEEE Transactions on Control Systems Technology*, vol. Submitted, 2008.